

Wasserstein Consensus ADMM

Iman Nadozi*

Abhishek Halder†

Abstract

We introduce Wasserstein consensus alternating direction method of multipliers (ADMM) and its entropic-regularized version: Sinkhorn consensus ADMM, to solve measure-valued optimization problems with convex additive objectives. Several problems of interest in stochastic prediction and learning can be cast in this form of measure-valued convex additive optimization. The proposed algorithm generalizes a variant of the standard Euclidean ADMM to the space of probability measures but departs significantly from its Euclidean counterpart. In particular, we derive a two layer ADMM algorithm wherein the outer layer is a variant of consensus ADMM on the space of probability measures while the inner layer is a variant of Euclidean ADMM. The resulting computational framework is particularly suitable for solving Wasserstein gradient flows via distributed computation. We demonstrate the proposed framework using illustrative numerical examples.

1 Introduction

Let $\mathcal{P}_2(\mathcal{X})$ denote the space of Borel probability measures over $\mathcal{X} \subseteq \mathbb{R}^d$ with finite second moments. Let $\mathcal{P}_{2,\text{ac}}(\mathcal{X}) := \{\mu \in \mathcal{P}_2(\mathcal{X}) \mid \mu \text{ is absolutely continuous w.r.t. the Lebesgue measure}\} \subset \mathcal{P}_2(\mathcal{X})$. A probability measure $\mu \in \mathcal{P}_{2,\text{ac}}(\mathcal{X})$ admits a joint probability density function (PDF) $\rho(\mathbf{x}) := \frac{d\mu}{d\mathbf{x}}$ such that $\rho \geq 0$ for all $\mathbf{x} \in \mathcal{X}$ and $\int_{\mathcal{X}} \rho \, d\mathbf{x} = 1$.

We consider measure-valued optimization problems of the form

$$\arg \inf_{\mu \in \mathcal{P}_2(\mathcal{X})} F(\mu) \quad (1)$$

where the objective F is expressible as a sum: $F(\mu) = F_1(\mu) + F_2(\mu) + \dots + F_n(\mu)$ for some finite $n \in \mathbb{N}, n > 1$. We suppose that the summand functionals $F_i : \mathcal{P}_2(\mathcal{X}) \mapsto (-\infty, +\infty]$ are proper lower semi-continuous (lsc), and convex along the generalized geodesics w.r.t. the 2-Wasserstein distance (Ambrosio et al., 2008, Ch. 9) for all $i \in [n]$. We will review the relevant technical preliminaries in Sec. 2. The purpose of this work is to design distributed algorithms to solve such measure-valued optimization problems with additive objective.

Instances of (1) are often encountered in machine learning (Chizat & Bach, 2018; Mei et al., 2018; Sirignano & Spiliopoulos, 2020; Zhang et al., 2018; Domingo-Enrich et al., 2020; Bunne et al., 2022) and control (Caluya & Halder, 2019, 2021). Most existing algorithms (Peyré, 2015; Benamou et al., 2016; Carlier et al., 2017; Wibisono, 2018; Alvarez-Melis et al., 2021; Mokrov et al., 2021; Kent et al., 2021; Carrillo et al., 2022; Fan et al., 2022; Wang & Li, 2022) for this class of problems require centralized computation; relatively few works (Dvurechenskii et al., 2018; Arqué et al., 2022) are available on solving specific instances of (1) via distributed computation. The main contribution of this work is to deduce a distributed algorithm for solving (1) by generalizing the Euclidean consensus ADMM to Wasserstein spaces. Our proposed algorithm realizes measure-valued operator

*Department of Electrical and Computer Engineering, University of California, Santa Cruz, inadozi@ucsc.edu

†Department of Applied Mathematics, University of California, Santa Cruz, ahalder@ucsc.edu

splitting (Bowles & Agueh, 2015; Bernton, 2018; Gallouët & Monsaingeon, 2017) but allows explicit distributed updates.

Motivation and Contributions. While problem (1) appears across many disciplines, one particular motivation behind our work is to numerically solve the *transient* solutions for measure-valued PDE initial value problems (IVPs). These PDEs are often nonlinear and nonlocal (see e.g., the second case study in Sec. 5), and difficult to solve scalably via traditional scientific computing methods such as finite difference. However, it is known that the flow induced by such PDE IVPs can often be seen (Ambrosio et al., 2008, Ch. 11), (Santambrogio, 2017) as gradient descent of a suitable free energy Lyapunov functional $F(\mu)$ w.r.t. the 2-Wasserstein metric over the space of measures. Then, high-level idea is to leverage this variational reformulation to compute the transient solutions for such IVPs by numerically performing Wasserstein gradient descent on (1).

The specific idea in this work is to further recognize that the functional F in practice has an additive structure $F(\cdot) = F_1(\cdot) + \dots + F_n(\cdot)$, which comes from different spatial operators (e.g., advection, interaction, diffusion) appearing in the PDE. One of our contribution here is to show that it is possible to leverage this additive structure in F to generalize the Euclidean ADMM to the Wasserstein space. The proposed algorithm can then be seen as a nonlinear superposition principle where different computers solve different (simpler) PDE IVPs by performing proximal update on a modified version of F_i , and then combine the resulting updates in a nonlinear manner. Historically, this point of view is very close to the origin of operator splitting (Glowinski & Le Tallec, 1989; Glowinski et al., 2016) in the PDE community that motivated the development of ADMM (Gabay & Mercier, 1976), albeit in the finite-dimensional setting.

We clarify here that while augmented Lagrangian methods for infinite dimensional problems have been investigated before, they appeared in the Hilbert spaces (Ito & Kunisch, 1990) or reflexive Banach spaces (Butnariu & Iusem, 2000; Kanzow et al., 2018). In contrast, the definition (16) for the Wasserstein augmented Lagrangian is novel. Our development is also different from the (standard) augmented Lagrangian for Wasserstein gradient flow as in (Benamou et al., 2016, equation 2.12), and directly works on the Wasserstein space.

2 Preliminaries

Wasserstein space and Wasserstein gradient flow. Let $\mathcal{B}(\mathcal{X})$ denote the Borel σ -field over $\mathcal{X} \subseteq \mathbb{R}^d$. For $\mu \in \mathcal{P}_2(\mathcal{X})$, and for any measurable map T defined on $(\mathcal{X}, \mathcal{B}(\mathcal{X}))$, let $T_{\#}\mu$ denote the pushforward a.k.a. transport of the probability measure μ via T .

For $\mathcal{X}, \mathcal{Y} \subseteq \mathbb{R}^d$, the *squared 2-Wasserstein distance* between a pair of probability measures $\mu_x \in \mathcal{P}_2(\mathcal{X})$, $\mu_y \in \mathcal{P}_2(\mathcal{Y})$, is defined as

$$W^2(\mu_x, \mu_y) := \inf_{\pi \in \Pi(\mu_x, \mu_y)} \int_{\mathcal{X} \times \mathcal{Y}} c(\mathbf{x}, \mathbf{y}) \, d\pi(\mathbf{x}, \mathbf{y}), \quad (2)$$

where $\Pi(\mu_x, \mu_y)$ is the set of joint probability measures or couplings over the product space $\mathcal{X} \times \mathcal{Y} \subseteq \mathbb{R}^{2d}$, having \mathbf{x} marginal μ_x , and \mathbf{y} marginal μ_y . Throughout, we use the ground cost $c(\mathbf{x}, \mathbf{y}) := \|\mathbf{x} - \mathbf{y}\|_2^2$ (the squared Euclidean distance) for $\mathbf{x} \in \mathcal{X}$, $\mathbf{y} \in \mathcal{Y}$. To lighten nomenclature, we henceforth refer to (2) as the “squared Wasserstein distance” dropping the prefix 2.

It is well-known (Villani, 2003, Ch. 7) that the Wasserstein distance W defines a metric on $\mathcal{P}_2(\mathcal{X})$. The minimizer of the linear program (2), denoted as π^{opt} , is referred to as the *optimal transportation plan*. If $\mu \in \mathcal{P}_{2, \text{ac}}(\mathcal{X})$, then π^{opt} is supported on the graph of the *optimal transport map* T^{opt} pushing μ_x to μ_y . We can rewrite (2) as

$$W^2(\mu_x, \mu_y) = \inf_{\text{Measurable } T: T_{\#}\mu_x = \mu_y} \int_{\mathcal{X}} c(\mathbf{x}, T(\mathbf{x})) \, d\mu_x, \quad (3)$$

and for the ground cost $c(\mathbf{x}, \mathbf{y}) := \|\mathbf{x} - \mathbf{y}\|_2^2$, the $\arg \inf$ for (3) is precisely T^{opt} that is unique a.e. (Brenier, 1991). We refer to $(\mathcal{P}_2(\mathcal{X}), W)$ as the *Wasserstein space* since it allows to define a Riemannian-like geometry. In particular, letting $L^2(\mu)$ denote the space of functions from $(\mathcal{X}, \mathcal{B}(\mathcal{X}))$ to $(\mathcal{Y}, \mathcal{B}(\mathcal{Y}))$, which are square integrable w.r.t. $\mu \in \mathcal{P}_2(\mathcal{X})$, we define the tangent space of $(\mathcal{P}_2(\mathcal{X}), W)$ at $\mu \in \mathcal{P}_2(\mathcal{X})$ as

$$\mathcal{T}_{\mu}\mathcal{P}_2(\mathcal{X}) := \overline{\{\nabla\phi \mid \phi \in C_c^{\infty}(\mathcal{X})\}},$$

where the overline denotes closure w.r.t. $L^2(\mu)$; see e.g., (Villani, 2009, Ch. 13).

A proper lsc functional $\Phi : \mathcal{P}_2(\mathcal{X}) \mapsto (-\infty, +\infty]$ is said to be *convex along generalized geodesics defined by the 2-Wasserstein distance* (Ambrosio et al., 2008, Ch. 9), if for any $t \in [0, 1]$ and any $\mu_1, \mu_2 \in \mathcal{P}_2(\mathcal{X})$, $\mu_3 \in \mathcal{P}_{2,ac}(\mathcal{X})$, we have

$$\Phi \left((tT_{3 \rightarrow 1}^{\text{opt}} + (1-t)T_{3 \rightarrow 2}^{\text{opt}})_{\#} \mu_3 \right) \leq t\Phi(\mu_1) + (1-t)\Phi(\mu_2),$$

where $T_{3 \rightarrow 1}^{\text{opt}}$ and $T_{3 \rightarrow 2}^{\text{opt}}$ are the optimal transport maps pushing μ_3 forward to μ_1 , and μ_3 forward to μ_2 , respectively. The measure-valued curve $t \mapsto (tT_{3 \rightarrow 1}^{\text{opt}} + (1-t)T_{3 \rightarrow 2}^{\text{opt}})_{\#} \mu_3$ interpolates between $\mu_2(t=0)$ and $\mu_1(t=1)$.

Given proper lsc $\Phi : \mathcal{P}_2(\mathcal{X}) \mapsto (-\infty, +\infty]$, its strong Fréchet subdifferential $\mu \mapsto \partial\Phi(\mu)$ allows defining the *Wasserstein gradient flow* (WGF) of the functional Φ , see e.g., (Ambrosio et al., 2008, Ch. 11), (Villani, 2009, Ch. 23), (Santambrogio, 2017). Additionally, when Φ is convex along generalized geodesics mentioned before, then the WGF can be characterized as the continuity equation

$$\frac{\partial \mu}{\partial t} + \nabla \cdot (\mu \mathbf{v}(\mu)) = 0, \quad \mathbf{v}(\mu) \in \partial\Phi(\mu) \cap \mathcal{T}_{\mu}\mathcal{P}_2(\mathcal{X}) \Leftrightarrow \mathbf{v}(\mu) = \nabla \frac{\delta \Phi}{\delta \mu}, \quad (4)$$

where ∇ is the d dimensional Euclidean gradient operator, and $\frac{\delta}{\delta \mu}$ denotes the functional derivative w.r.t. μ . More generally, for non-smooth Φ , one can define WGF via Evolution Variational Inequality (EVI) (Ambrosio et al., 2008, Thm. 11.1.4), (Salim et al., 2020).

Following (4), we can formally define the Wasserstein gradient (Villani, 2003, Ch. 9.1), (Ambrosio et al., 2008, Ch. 8) as

$$\nabla^W \Phi(\mu) := -\nabla \cdot \left(\mu \nabla \frac{\delta \Phi}{\delta \mu} \right), \quad (5)$$

and express the WGF in the form

$$\frac{\partial \mu}{\partial t} = -\nabla^W \Phi(\mu). \quad (6)$$

In this work, we consider smooth Φ with singleton $\partial\Phi(\mu) = \{\nabla^W \Phi(\mu)\}$ (Ambrosio et al., 2008, Ch. 10.4).

Sinkhorn regularization. For $\pi \in \Pi(\mu_x, \mu_y)$ and a reference probability measure π_0 supported over $\mathcal{X} \times \mathcal{Y}$, the notation $\pi \ll \pi_0$ means that π is absolutely continuous w.r.t. π_0 . Given a strictly convex regularizer $R(\cdot)$, define the *regularized squared Wasserstein distance*

$$W_{\varepsilon}^2(\mu_x, \mu_y) := \inf_{\substack{\pi \in \Pi(\mu_x, \mu_y) \\ \pi \ll \pi_0}} \int_{\mathcal{X} \times \mathcal{Y}} c(\mathbf{x}, \mathbf{y}) \, d\pi(\mathbf{x}, \mathbf{y}) + \varepsilon \int_{\mathcal{X} \times \mathcal{Y}} R\left(\frac{d\pi}{d\pi_0}\right) d\pi_0(\mathbf{x}, \mathbf{y}) \quad (7)$$

where $\varepsilon > 0$ is a regularization parameter, and $\frac{d\pi}{d\pi_0}$ denotes the Radon-Nikodym derivative. Examples of π_0 include the product measure $\mu_x(\mathbf{x})\mu_y(\mathbf{y})$ (Genevay et al., 2016) and the uniform measure (Cuturi, 2013). In this paper, we consider the entropic regularizer

$$R(x) := x \log x - x \quad \text{for } x \geq 0, \quad \text{with the convention } 0 \log 0 = 0. \quad (8)$$

The work in (Cuturi, 2013) considered the discrete version of (7) with an entropic regularizer R as above, and named it as the *Sinkhorn divergence*. This entropy or Sinkhorn regularized squared Wasserstein distance has found widespread applications in the computation and analysis of variational problems involving the Wasserstein distance (see e.g., Benamou et al. (2015); Carlier et al. (2017); Peyré (2015); Cuturi & Peyré (2016)), and will be useful in our development too.

Wasserstein barycenter. Given the measures $\mu_1, \dots, \mu_n \in \mathcal{P}_2(\mathcal{X})$ and positive weights w_1, \dots, w_n , the *Wasserstein barycenter* (Agueh & Carlier, 2011) is given by

$$\arg \inf_{\mu \in \mathcal{P}_2(\mathcal{X})} \sum_{i=1}^n w_i W^2(\mu, \mu_i). \quad (9)$$

In (9), replacing W^2 by W_ε^2 defined in (7) with R as in (8), results in the *Sinkhorn regularized Wasserstein barycenter*

$$\arg \inf_{\mu \in \mathcal{P}_2(\mathcal{X})} \sum_{i=1}^n w_i W_\varepsilon^2(\mu, \mu_i). \quad (10)$$

Wasserstein proximal operator. We use the notation $\text{prox}_{G(\cdot)}^W(\zeta)$ to denote the *Wasserstein proximal operator* of proper lsc $G : \mathcal{P}_2(\mathcal{X}) \mapsto (-\infty, +\infty]$, acting on $\zeta \in \mathcal{P}_2(\mathcal{X})$, given by

$$\text{prox}_{G(\cdot)}^W(\zeta) := \arg \inf_{\mu \in \mathcal{P}_2(\mathcal{X})} \frac{1}{2} W^2(\mu, \zeta) + G(\mu). \quad (11)$$

The Wasserstein proximal operator (11) can be seen as a generalization of the finite dimensional Euclidean proximal operator of proper lsc $g : \mathbb{R}^d \mapsto (-\infty, +\infty]$, given by

$$\text{prox}_g^{\|\cdot\|_2}(\mathbf{z}) := \arg \inf_{\mathbf{x} \in \mathbb{R}^d} \frac{1}{2} \|\mathbf{x} - \mathbf{z}\|_2^2 + g(\mathbf{x}). \quad (12)$$

Wasserstein proximal operators of the form (11) go back to the seminal work of Jordan et al. (1998), and have been used in stochastic prediction (Caluya & Halder, 2019), control (Caluya & Halder, 2021), learning (Chu et al., 2019; Frogner & Poggio, 2020; Salim et al., 2020; Mokrov et al., 2021), and in modeling of population dynamics (Bunne et al., 2022).

Legendre-Fenchel conjugate. The Legendre-Fenchel conjugate of a real-valued function f is

$$f^*(\mathbf{y}) := \sup_{\mathbf{x} \in \text{domain}(f)} (\langle \mathbf{y}, \mathbf{x} \rangle - f(\mathbf{x})),$$

where $\langle \cdot, \cdot \rangle$ denotes the standard inner product. The function f^* is convex even if f is not. When $f(\mathbf{x}) = \langle \mathbf{a}, \mathbf{x} \rangle$, $\mathbf{a} \in \mathbb{R}^d \setminus \{\mathbf{0}\}$, then $f^*(\mathbf{y})$ is the indicator function of the singleton $\{\mathbf{a}\}$, i.e.,

$$f^*(\mathbf{y}) = \begin{cases} 0 & \text{if } \mathbf{y} = \mathbf{a}, \\ +\infty & \text{otherwise.} \end{cases} \quad (13)$$

ADMM. The constrained optimization problem $\min_{\mathbf{x} \in \mathbb{R}^N} f(\mathbf{x})$ subject to $\mathbf{x} \in \mathcal{C} \subset \mathbb{R}^N$, where the function f and the set \mathcal{C} are convex, can be re-written as $\min_{\mathbf{x}, \mathbf{z} \in \mathbb{R}^N} f(\mathbf{x}) + \mathbf{1}_{\mathcal{C}}(\mathbf{z})$ subject to $\mathbf{x} = \mathbf{z}$ where the indicator function $\mathbf{1}_{\mathcal{C}}(\mathbf{z}) := 0$ if $\mathbf{z} \in \mathcal{C}$, and $\mathbf{1}_{\mathcal{C}}(\mathbf{z}) := +\infty$ if $\mathbf{z} \notin \mathcal{C}$. Denote the dual variable associated with the constraint $\mathbf{x} = \mathbf{z}$ as $\boldsymbol{\nu} \in \mathbb{R}^N$, and let $\tilde{\boldsymbol{\nu}} := \boldsymbol{\nu}/\tau$ be the scaled dual variable for some parameter $\tau > 0$. The augmented Lagrangian for this problem is $L_\tau(\mathbf{x}, \mathbf{z}, \tilde{\boldsymbol{\nu}}) := f(\mathbf{x}) + \mathbf{1}_{\mathcal{C}}(\mathbf{z}) + \frac{\tau}{2} \|\mathbf{x} - \mathbf{z} + \tilde{\boldsymbol{\nu}}\|_2^2$. Each iteration of the ADMM algorithm in the so-called ‘‘scaled form’’ (Boyd et al., 2011, Ch. 5), comprises of the following three steps:

$$\mathbf{x}^{k+1} = \arg \min_{\mathbf{x} \in \mathbb{R}^N} f(\mathbf{x}) + \frac{\tau}{2} \|\mathbf{x} - \mathbf{z}^k + \tilde{\boldsymbol{\nu}}^k\|_2^2 \stackrel{(12)}{=} \text{prox}_{\frac{1}{\tau}f}^{\|\cdot\|_2}(\mathbf{z}^k - \tilde{\boldsymbol{\nu}}^k), \quad (14a)$$

$$\mathbf{z}^{k+1} = \text{proj}_{\mathcal{C}}(\mathbf{x}^{k+1} + \tilde{\boldsymbol{\nu}}^k), \quad (14b)$$

$$\tilde{\boldsymbol{\nu}}^{k+1} = \tilde{\boldsymbol{\nu}}^k + (\mathbf{x}^{k+1} - \mathbf{z}^{k+1}), \quad (14c)$$

where the iteration index $k \in \mathbb{N}_0$ (the set of whole numbers $\{0, 1, 2, \dots\}$), and $\text{proj}_{\mathcal{C}}$ denotes the Euclidean projection onto \mathcal{C} . The steps (14a)-(14b) involve alternating minimization of the augmented Lagrangian L_τ , and the step (14c) involves dual ascent. Notice that in the scaled form ADMM, the parameter τ *does not* appear in (14c) as the pre-factor of the term in parenthesis. For ADMM convergence results, see e.g., (Nishihara et al., 2015), (Wang et al., 2019).

For a separable objective $f(\mathbf{x}_1, \dots, \mathbf{x}_n) = \sum_{i=1}^n f_i(\mathbf{x}_i)$, where $\mathbf{x}_i \in \mathbb{R}^N$ and f_i convex for all $i \in [n]$,

it is immediate from (14) that the updates (14a) and (14c) can be parallelized across the index $i \in [n]$. The nature of computation in step (14b) depends on the constraint set \mathcal{C} , see e.g., (Parikh & Boyd, 2014, Ch. 5). For instance, if \mathcal{C} is the consensus constraint $\mathbf{x}_1 = \dots = \mathbf{x}_n = \mathbf{z}$, then (14b) requires an averaging of the local updates, resulting in a ‘‘broadcast and gather’’ computation. In Sec. 4.2, we will encounter an instance of (14) that will admit parallelization.

3 Main Idea

To leverage the additive structure of the objective in (1) for distributed computation, we start by rewriting it in the consensus form. Specifically, we relabel the argument of the functional F_i as μ_i for all $i \in [n]$, and then impose the consensus constraint $\mu_1 = \mu_2 = \dots = \mu_n$. Letting $\mathcal{P}_2^{n+1}(\mathcal{X}) := \underbrace{\mathcal{P}_2(\mathcal{X}) \times \dots \times \mathcal{P}_2(\mathcal{X})}_{n+1 \text{ times}}$, we thus transcribe (1) into

$$\arg \inf_{(\mu_1, \dots, \mu_n, \zeta) \in \mathcal{P}_2^{n+1}(\mathcal{X})} F_1(\mu_1) + F_2(\mu_2) + \dots + F_n(\mu_n) \quad (15a)$$

$$\text{subject to } \mu_i = \zeta \quad \text{for all } i \in [n]. \quad (15b)$$

Denote an element of the base space as $\boldsymbol{\theta} \in \mathcal{X} \subseteq \mathbb{R}^d$. Akin to the standard (Euclidean) augmented Lagrangian, we define the *Wasserstein augmented Lagrangian*

$$L_\alpha(\mu_1, \dots, \mu_n, \zeta, \nu_1, \dots, \nu_n) := \sum_{i=1}^n \left\{ F_i(\mu_i) + \frac{\alpha}{2} W^2(\mu_i, \zeta) + \int_{\mathcal{X}} \nu_i(\boldsymbol{\theta}) (\mathrm{d}\mu_i - \mathrm{d}\zeta) \right\} \quad (16)$$

where $\nu_i(\boldsymbol{\theta})$, $i \in [n]$, are the Lagrange multipliers for the constraints in (15b), and $\alpha > 0$ is a regularization constant.

Motivated by the Euclidean ADMM, we then set up the recursions

$$\mu_i^{k+1} = \arg \inf_{\mu_i \in \mathcal{P}_2(\mathcal{X})} L_\alpha(\mu_1, \dots, \mu_n, \zeta^k, \nu_1^k, \dots, \nu_n^k) \quad (17a)$$

$$\zeta^{k+1} = \arg \inf_{\zeta \in \mathcal{P}_2(\mathcal{X})} L_\alpha(\mu_1^{k+1}, \dots, \mu_n^{k+1}, \zeta, \nu_1^k, \dots, \nu_n^k) \quad (17b)$$

$$\nu_i^{k+1} = \nu_i^k + \alpha (\mu_i^{k+1} - \zeta^{k+1}) \quad (17c)$$

where $i \in [n]$, and the recursion index $k \in \mathbb{N}_0$. It will be useful to introduce

$$\nu_{\text{sum}}^k(\boldsymbol{\theta}) := \sum_{i=1}^n \nu_i^k(\boldsymbol{\theta}), \quad k \in \mathbb{N}_0. \quad (18)$$

We view (17a)-(17b) as primal updates, and (17c) as dual ascent.

Substituting (16) in (17), dropping the terms independent of the decision variable in the respective arg inf, re-scaling, and using (18), the recursions (17) simplify to

$$\begin{aligned} \mu_i^{k+1} &= \arg \inf_{\mu_i \in \mathcal{P}_2(\mathcal{X})} \frac{1}{2} W^2(\mu_i, \zeta^k) + \frac{1}{\alpha} \left\{ F_i(\mu_i) + \int_{\mathcal{X}} \nu_i^k(\boldsymbol{\theta}) \mathrm{d}\mu_i \right\} \\ &= \text{prox}_{\frac{1}{\alpha}}^{W^2} (F_i(\cdot) + \int \nu_i^k \mathrm{d}(\cdot)) (\zeta^k), \end{aligned} \quad (19a)$$

$$\begin{aligned} \zeta^{k+1} &= \arg \inf_{\zeta \in \mathcal{P}_2(\mathcal{X})} \sum_{i=1}^n \left\{ \frac{1}{2} W^2(\mu_i^{k+1}, \zeta) - \frac{1}{\alpha} \int_{\mathcal{X}} \nu_i^k(\boldsymbol{\theta}) \mathrm{d}\zeta \right\} \\ &= \arg \inf_{\zeta \in \mathcal{P}_2(\mathcal{X})} \left\{ \left(\sum_{i=1}^n W^2(\mu_i^{k+1}, \zeta) \right) - \frac{2}{\alpha} \int_{\mathcal{X}} \nu_{\text{sum}}^k(\boldsymbol{\theta}) \mathrm{d}\zeta \right\}, \end{aligned} \quad (19b)$$

$$\nu_i^{k+1} = \nu_i^k + \alpha (\mu_i^{k+1} - \zeta^{k+1}). \quad (19c)$$

We refer to (19) as the *Wasserstein consensus ADMM* generalizing its finite dimensional Euclidean counterpart in the sense (19a)-(19b) are analogues of the so-called x and z updates, respectively (Parikh & Boyd, 2014, Ch. 5.2.1). However, important difference arises in (19b) compared to its Euclidean counterpart due to the sum of squares of Wasserstein distances. In the Euclidean case, the corresponding z update can be analytically performed in terms of the *arithmetic mean* of the x updates. While (19b) involves a *generalized mean* of the updates from (19a), we now have *Wasserstein barycentric proximal* of a linear functional in ν_{sum}^k w.r.t. n measures $\{\mu_1^{k+1}, \dots, \mu_n^{k+1}\}$.

The proximal updates (19a) are closely related to the WGFs of the form (6) generated by the respective (scaled) free energy functionals

$$\Phi_i(\mu_i) := F_i(\mu_i) + \int_{\mathcal{X}} \nu_i^k \mathrm{d}\mu_i, \quad \mu_i \in \mathcal{P}_2(\mathcal{X}), \quad i \in [n]. \quad (20)$$

As per the assumptions on F_i , the functionals Φ_i are also proper lsc and convex along generalized geodesics defined by the 2-Wasserstein distance. As $1/\alpha \downarrow 0$, the sequence $\{\mu_i^k(\alpha)\}_{k \in \mathbb{N}_0}$ generated by the updates (19a) converge to the measure-valued solution trajectory $\tilde{\mu}_i(t, \cdot)$, $t \in [0, \infty)$ solving the initial value problem (IVP)

$$\frac{\partial \tilde{\mu}_i}{\partial t} = -\nabla^W \Phi_i(\tilde{\mu}_i), \quad \tilde{\mu}_i(t=0, \cdot) = \tilde{\mu}_i^0(\cdot), \quad i \in [n]. \quad (21)$$

Thus, in a rather generic setting, performing the proximal updates (19a) in parallel across the index $i \in [n]$, amounts to performing distributed time updates for the approximate transient solutions of the IVPs (21). In Appendix A, we provide important examples of (20)-(21). An interesting observation for (19a) is that for each $i \in [n]$, the dual variables ν_i^k contribute as time-varying advection potentials irrespective of whether F_i already has an advection potential or not.

Remark 1. Notice that the Lagrange multiplier ν_i for the i^{th} measure consensus constraint (15b) must be an element of the dual space of \mathcal{P}_2 comprising of bounded linear functionals of the elements of \mathcal{P}_2 . Thus, when the primal updates for μ_i are identified with the corresponding WGFs, then the Lagrange multipliers ν_i become "algorithmic" advection potentials. For the same reason, the integral involving the Lagrange multiplier ends up being simply an Euclidean inner product post-discretization; see (22).

In the next Section, we propose a two-layer ADMM algorithm (see Fig. 1) to solve (19).

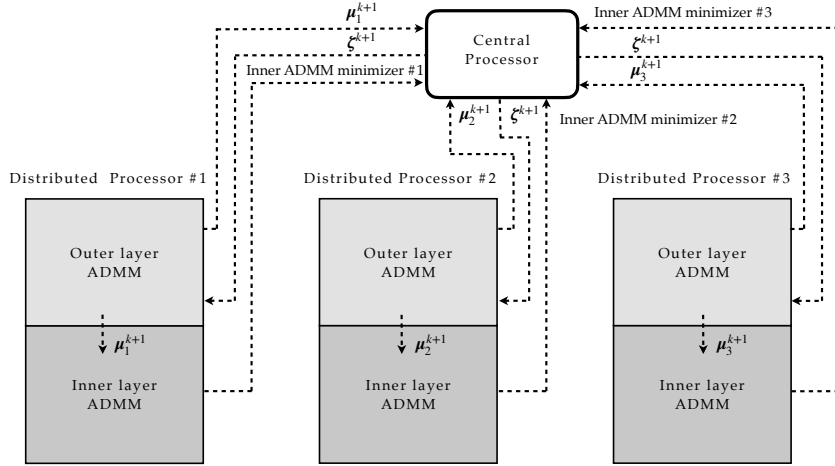


Figure 1: High level schematic of the proposed two-layer ADMM algorithm illustrated with one central and $n = 3$ distributed processors. The central processor updates ζ^{k+1} . The “upstairs” (lighter shade) of the distributed processors update μ_i^{k+1} via *outer layer ADMM* (Sec. 4.1). These distributed μ_i^{k+1} updates and the centralized ζ^{k+1} values are passed to the “downstairs” (darker shade) of the distributed processors for updating ζ^{k+1} via an *inner layer ADMM* (Sec. 4.2).

4 Results

To numerically realize the recursions (19), we consider a sequence of discrete probability distributions $\{\mu_1^k, \dots, \mu_n^k, \zeta^k\}_{k \in \mathbb{N}_0}$ where each distribution is a probability vector of length $N \times 1$ comprising respective probability values at N samples. Thus, for each fixed $k \in \mathbb{N}_0$, the tuple

$$(\mu_1^k, \dots, \mu_n^k, \zeta^k) \in \underbrace{\Delta^{N-1} \times \dots \times \Delta^{N-1}}_{n+1 \text{ times}} =: (\Delta^{N-1})^{n+1} \quad (\text{the product simplex}).$$

Likewise, for each $k \in \mathbb{N}_0$, the multipliers $(\nu_1^k, \dots, \nu_n^k) \in \mathbb{R}^{nN}$, and $\nu_{\text{sum}}^k = \sum_{i=1}^n \nu_i^k \in \mathbb{R}^N$.

Given probability vectors $\xi, \eta \in \Delta^{N-1}$, let $\Pi_N(\xi, \eta) := \{M \in \mathbb{R}^{N \times N} \mid M \geq 0 \text{ (elementwise)}, M\mathbf{1} = \xi, M^\top \mathbf{1} = \eta\}$. Also, let $C \in \mathbb{R}^{N \times N}$ denote the squared Eu-

clidean distance matrix for the sampled data $\{\boldsymbol{\theta}_r\}_{r \in [N]}$ in \mathbb{R}^d , i.e., the entries of the matrix \mathbf{C} are $\mathbf{C}(i, j) := \|\boldsymbol{\theta}_i - \boldsymbol{\theta}_j\|_2^2$ for all $i, j \in [N]$.

For each $i \in [n]$ and $k \in \mathbb{N}_0$, we write the discrete version of (19) as

$$\begin{aligned} \boldsymbol{\mu}_i^{k+1} &= \text{prox}_{\frac{1}{\alpha}(F_i(\boldsymbol{\mu}_i) + \langle \boldsymbol{\nu}_i^k, \boldsymbol{\mu}_i \rangle)}^W(\boldsymbol{\zeta}^k) \\ &= \arg \inf_{\boldsymbol{\mu}_i \in \Delta^{N-1}} \left\{ \min_{\mathbf{M} \in \Pi_N(\boldsymbol{\mu}_i, \boldsymbol{\zeta}^k)} \frac{1}{2} \langle \mathbf{C}, \mathbf{M} \rangle + \frac{1}{\alpha} (F_i(\boldsymbol{\mu}_i) + \langle \boldsymbol{\nu}_i^k, \boldsymbol{\mu}_i \rangle) \right\}, \end{aligned} \quad (22a)$$

$$\boldsymbol{\zeta}^{k+1} = \arg \inf_{\boldsymbol{\zeta} \in \Delta^{N-1}} \left\{ \left(\sum_{i=1}^n \min_{\mathbf{M}_i \in \Pi_N(\boldsymbol{\mu}_i^{k+1}, \boldsymbol{\zeta})} \frac{1}{2} \langle \mathbf{C}, \mathbf{M}_i \rangle \right) - \frac{2}{\alpha} \langle \boldsymbol{\nu}_{\text{sum}}^k, \boldsymbol{\zeta} \rangle \right\}, \quad (22b)$$

$$\boldsymbol{\nu}_i^{k+1} = \boldsymbol{\nu}_i^k + \alpha (\boldsymbol{\mu}_i^{k+1} - \boldsymbol{\zeta}^{k+1}), \quad (22c)$$

wherein (22a)-(22b) used the discrete version of (2).

Replacing the squared Wasserstein distance (2) in (19) by its Sinkhorn regularized version (7), modify the recursions (22) as

$$\begin{aligned} \boldsymbol{\mu}_i^{k+1} &= \text{prox}_{\frac{1}{\alpha}(F_i(\boldsymbol{\mu}_i) + \langle \boldsymbol{\nu}_i^k, \boldsymbol{\mu}_i \rangle)}^{W_\varepsilon}(\boldsymbol{\zeta}^k) \\ &= \arg \inf_{\boldsymbol{\mu}_i \in \Delta^{N-1}} \left\{ \min_{\mathbf{M} \in \Pi_N(\boldsymbol{\mu}_i, \boldsymbol{\zeta}^k)} \left\langle \frac{1}{2} \mathbf{C} + \varepsilon \log \mathbf{M}, \mathbf{M} \right\rangle + \frac{1}{\alpha} (F_i(\boldsymbol{\mu}_i) + \langle \boldsymbol{\nu}_i^k, \boldsymbol{\mu}_i \rangle) \right\}, \end{aligned} \quad (23a)$$

$$\boldsymbol{\zeta}^{k+1} = \arg \inf_{\boldsymbol{\zeta} \in \Delta^{N-1}} \left\{ \left(\sum_{i=1}^n \min_{\mathbf{M}_i \in \Pi_N(\boldsymbol{\mu}_i^{k+1}, \boldsymbol{\zeta})} \left\langle \frac{1}{2} \mathbf{C} + \varepsilon \log \mathbf{M}_i, \mathbf{M}_i \right\rangle \right) - \frac{2}{\alpha} \langle \boldsymbol{\nu}_{\text{sum}}^k, \boldsymbol{\zeta} \rangle \right\}, \quad (23b)$$

$$\boldsymbol{\nu}_i^{k+1} = \boldsymbol{\nu}_i^k + \alpha (\boldsymbol{\mu}_i^{k+1} - \boldsymbol{\zeta}^{k+1}), \quad (23c)$$

where $\varepsilon > 0$ is a regularization parameter.

Remark 2. For $\varepsilon \downarrow 0$, the solution of the inner minimization (23a) is known (Peyré, 2015, Sec. 3) to be a consistent approximation of that in (22a). The Wasserstein proximal update (22a) can, in principle, be performed by the proximal gradient Jordan-Kinderlehrer-Otto (JKO) algorithm as in (Salim et al., 2020) with more general regularization. Our motivation for choosing Sinkhorn regularization is computational convenience. As we explain in Sec. 4.1, when we dualize the inner minimization problem in (23a), not only we have strong duality, but we also can explicitly write the proximal update in terms of multipliers which can be obtained, in general, numerically via provably contractive block-coordinate ascent. Note that (Salim et al., 2020, Remark 1) mentions the computational convenience of performing the JKO update for the negative entropy regularization.

Remark 3. While there exists prior work such as (Yang et al., 2021) for unregularized computation of the Wasserstein barycenter using multi-block ADMM, the nested minimization in (22b) is different from computing barycenter in that it involves computing the Wasserstein barycentric proximal.

We next provide novel results and algorithmic details to numerically perform the recursions (23).

4.1 The $\boldsymbol{\mu}$ Update

The Sinkhorn regularized recursions (23a) comprise the outer layer ADMM in Fig. 1. These recursions allow us to get semi-analytical handle on the nested minimization via strong duality. Specifically, consider the (proper lsc and convex w.r.t. generalized geodesic) functionals $F_i, G_i : \Delta^{N-1} \mapsto \mathbb{R}$ for all $i \in [n]$, where

$$G_i(\boldsymbol{\mu}_i) := F_i(\boldsymbol{\mu}_i) + \langle \boldsymbol{\nu}_i^k, \boldsymbol{\mu}_i \rangle, \quad (24)$$

and denote the Legendre-Fenchel conjugate of G_i as G_i^* . Following (Karlsson & Ringh, 2017, Lemma 3.5), (Caluya & Halder, 2019, Sec. III), the Lagrange dual problem associated with (23a), for each $i \in [n]$, is

$$(\boldsymbol{\lambda}_{0i}^{\text{opt}}, \boldsymbol{\lambda}_{1i}^{\text{opt}}) = \arg \max_{\boldsymbol{\lambda}_{0i}, \boldsymbol{\lambda}_{1i} \in \mathbb{R}^N} \left\{ \langle \boldsymbol{\lambda}_{0i}, \boldsymbol{\zeta}^k \rangle - G_i^*(-\boldsymbol{\lambda}_{1i}) - \alpha \varepsilon \left(\exp \left(\frac{\boldsymbol{\lambda}_{0i}^\top}{\alpha \varepsilon} \right) \exp \left(-\frac{\mathbf{C}}{2\varepsilon} \right) \exp \left(\frac{\boldsymbol{\lambda}_{1i}}{\alpha \varepsilon} \right) \right) \right\}. \quad (25)$$

Using (25), the proximal updates in (23a) can be recovered³ via the following Proposition.

Proposition 1. (Karlsson & Ringh, 2017, Lemma 3.5),(Caluya & Halder, 2019, Theorem 1) Given $\alpha, \varepsilon > 0$, the squared Euclidean distance matrix $\mathbf{C} \in \mathbb{R}^{N \times N}$, and the probability vector $\boldsymbol{\zeta}^k \in \Delta^{N-1}$, $k \in \mathbb{N}_0$. Let $\mathbf{0}$ denote the $N \times 1$ vector of zeros. For $i \in [n]$, the vectors $\boldsymbol{\lambda}_{0i}^{\text{opt}}, \boldsymbol{\lambda}_{1i}^{\text{opt}} \in \mathbb{R}^N$ in (25) solve the system

$$\exp\left(\frac{\boldsymbol{\lambda}_{0i}^{\text{opt}}}{\alpha\varepsilon}\right) \odot \left(\exp\left(-\frac{\mathbf{C}}{2\varepsilon}\right) \exp\left(\frac{\boldsymbol{\lambda}_{1i}^{\text{opt}}}{\alpha\varepsilon}\right)\right) = \boldsymbol{\zeta}_k, \quad (26a)$$

$$\mathbf{0} \in \partial_{\boldsymbol{\lambda}_{1i}^{\text{opt}}} G_i^*(-\boldsymbol{\lambda}_{1i}^{\text{opt}}) - \exp\left(\frac{\boldsymbol{\lambda}_{1i}^{\text{opt}}}{\alpha\varepsilon}\right) \odot \left(\exp\left(-\frac{\mathbf{C}^\top}{2\varepsilon}\right) \exp\left(\frac{\boldsymbol{\lambda}_{0i}^{\text{opt}}}{\alpha\varepsilon}\right)\right). \quad (26b)$$

The proximal update $\boldsymbol{\mu}_i^{k+1}$ in (23a) is given by

$$\boldsymbol{\mu}_i^{k+1} = \exp\left(\frac{\boldsymbol{\lambda}_{1i}^{\text{opt}}}{\alpha\varepsilon}\right) \odot \left(\exp\left(-\frac{\mathbf{C}^\top}{2\varepsilon}\right) \exp\left(\frac{\boldsymbol{\lambda}_{0i}^{\text{opt}}}{\alpha\varepsilon}\right)\right). \quad (27)$$

For a given F_i , in general, the pair $(\boldsymbol{\lambda}_{0i}^{\text{opt}}, \boldsymbol{\lambda}_{1i}^{\text{opt}})$ need to be computed numerically from (26); see various cases discussed in Appendix B. In particular, Theorem 2 of Appendix B, deduces that when F_i in (24) is a linear functional, then $(\boldsymbol{\lambda}_{0i}^{\text{opt}}, \boldsymbol{\lambda}_{1i}^{\text{opt}})$, and thus $\boldsymbol{\mu}_i^{k+1}$, can in fact be computed analytically. This result will find use in our experiments in Sec. 5.

We next consider numerically realizing the update (23b).

4.2 The $\boldsymbol{\zeta}$ Update

The update (23b) concerns with computing the Sinkhorn regularized Wasserstein barycenter (see (10)) with an extra linear regularization. We have the following result (proof in Appendix C).

Theorem 1. Given $\alpha, \varepsilon > 0$, the squared Euclidean distance matrix $\mathbf{C} \in \mathbb{R}^{N \times N}$, and the probability vectors $\boldsymbol{\mu}_i^{k+1} \in \Delta^{N-1}$ for all $i \in [n]$, $k \in \mathbb{N}_0$, let $\boldsymbol{\Gamma} := \exp(-\mathbf{C}/2\varepsilon)$. Let

$$\begin{aligned} (\mathbf{u}_1^{\text{opt}}, \dots, \mathbf{u}_n^{\text{opt}}) &= \arg \min_{(\mathbf{u}_1, \dots, \mathbf{u}_n) \in \mathbb{R}^{nN}} \sum_{i=1}^n \langle \boldsymbol{\mu}_i^{k+1}, \log(\boldsymbol{\Gamma} \exp(\mathbf{u}_i/\varepsilon)) \rangle \\ &\text{subject to } \sum_{i=1}^n \mathbf{u}_i = \frac{2}{\alpha} \boldsymbol{\nu}_{\text{sum}}^k. \end{aligned} \quad (28)$$

Then, the update $\boldsymbol{\zeta}^{k+1}$ in (23b) is given by

$$\boldsymbol{\zeta}^{k+1} = \exp(\mathbf{u}_i^{\text{opt}}/\varepsilon) \odot (\boldsymbol{\Gamma} (\boldsymbol{\mu}_i^{k+1} \oslash (\boldsymbol{\Gamma} \exp(\mathbf{u}_i^{\text{opt}}/\varepsilon)))) \in \Delta^{N-1}, \quad \text{for all } i \in [n]. \quad (29)$$

We observe that (28) has a separable sum objective where each summand is a weighted log-sum-exp (thus convex). Denoting these summands as

$$f_i(\mathbf{u}_i) := \langle \boldsymbol{\mu}_i^{k+1}, \log(\boldsymbol{\Gamma} \exp(\mathbf{u}_i/\varepsilon)) \rangle, \quad \mathbf{u}_i \in \mathbb{R}^N, \quad \text{for all } i \in [n], \quad (30)$$

we write (28) in the scaled ADMM form (14):

$$\mathbf{u}_i^{\ell+1} = \text{prox}_{\frac{1}{\tau} f_i}^{\|\cdot\|_2}(\mathbf{z}_i^\ell - \tilde{\mathbf{v}}_i^\ell), \quad i \in [n], \quad (31a)$$

$$\mathbf{z}^{\ell+1} = \text{proj}_{\mathcal{C}}(\mathbf{u}^{\ell+1} + \tilde{\mathbf{v}}^\ell), \quad (31b)$$

$$\tilde{\mathbf{v}}_i^{\ell+1} = \tilde{\mathbf{v}}_i^\ell + (\mathbf{u}_i^{\ell+1} - \mathbf{z}_i^{\ell+1}), \quad i \in [n], \quad (31c)$$

where $\ell \in \mathbb{N}_0$ is the ADMM iteration index while holding the index k fixed, $\tau > 0$, and $\mathbf{u}^\ell := (\mathbf{u}_1^\ell, \dots, \mathbf{u}_n^\ell) \in \mathbb{R}^{nN}$, $\mathbf{z}^\ell := (\mathbf{z}_1^\ell, \dots, \mathbf{z}_n^\ell) \in \mathbb{R}^{nN}$, $\tilde{\mathbf{v}}^\ell := (\tilde{\mathbf{v}}_1^\ell, \dots, \tilde{\mathbf{v}}_n^\ell) \in \mathbb{R}^{nN}$ for all $\ell \in \mathbb{N}_0$. The constraint set \mathcal{C} in (31b) corresponds to the equality constraint in (28), i.e.,

$$\mathcal{C} := \left\{ (\mathbf{z}_1, \dots, \mathbf{z}_n) \in \mathbb{R}^{nN} \mid \mathbf{z}_1 + \dots + \mathbf{z}_n = \frac{2}{\alpha} \boldsymbol{\nu}_{\text{sum}}^k \right\}. \quad (32)$$

To proceed further, we need the following Lemma (proof in Appendix D).

³See Appendix B for examples.

Lemma 1. For any $\mathbf{v} := (\mathbf{v}_1, \dots, \mathbf{v}_n) \in \mathbb{R}^{nN}$, where the subvectors $\mathbf{v}_i \in \mathbb{R}^N$ for all $i \in [n]$, let $\bar{\mathbf{v}} := \frac{1}{n} \sum_{i=1}^n \mathbf{v}_i \in \mathbb{R}^N$. Then the Euclidean projection of \mathbf{v} onto \mathcal{C} in (32) is

$$\text{proj}_{\mathcal{C}}(\mathbf{v}) = \left(\mathbf{v}_1 - \bar{\mathbf{v}} + \frac{2}{n\alpha} \boldsymbol{\nu}_{\text{sum}}^k, \dots, \mathbf{v}_n - \bar{\mathbf{v}} + \frac{2}{n\alpha} \boldsymbol{\nu}_{\text{sum}}^k \right) \in \mathbb{R}^{nN}.$$

Thanks to Lemma 1, we can parallelize (31b) as

$$\mathbf{z}_i^{\ell+1} = \left(\mathbf{u}_i^{\ell+1} - \frac{1}{n} \sum_{i=1}^n \mathbf{u}_i^{\ell+1} \right) + \left(\tilde{\mathbf{v}}_i^\ell - \frac{1}{n} \sum_{i=1}^n \tilde{\mathbf{v}}_i^\ell \right) + \frac{2}{n\alpha} \boldsymbol{\nu}_{\text{sum}}^k, \quad i \in [n]. \quad (33)$$

Therefore, (28) can be solved in a distributed manner:

$$\mathbf{u}_i^{\ell+1} = \text{prox}_{\frac{1}{\tau} f_i}^{\|\cdot\|_2}(\mathbf{z}_i^\ell - \tilde{\mathbf{v}}_i^\ell), \quad i \in [n], \quad (34a)$$

$$\mathbf{z}_i^{\ell+1} = \left(\mathbf{u}_i^{\ell+1} - \frac{1}{n} \sum_{i=1}^n \mathbf{u}_i^{\ell+1} \right) + \left(\tilde{\mathbf{v}}_i^\ell - \frac{1}{n} \sum_{i=1}^n \tilde{\mathbf{v}}_i^\ell \right) + \frac{2}{n\alpha} \boldsymbol{\nu}_{\text{sum}}^k, \quad i \in [n], \quad (34b)$$

$$\tilde{\mathbf{v}}_i^{\ell+1} = \tilde{\mathbf{v}}_i^\ell + (\mathbf{u}_i^{\ell+1} - \mathbf{z}_i^{\ell+1}), \quad i \in [n]. \quad (34c)$$

The proximal update (34a) does not admit an analytical solution. To numerically compute (34a), we take advantage of the structured Hessian (see Appendix E) of the proximal objective and implement the Newton's method with variable step size computed by backtracking line search. The recursions (34) comprise the inner layer ADMM in Fig. 1.

4.3 Summary and Convergence

Fig. 5 in Appendix F provides a detailed schematic of the proposed algorithmic framework, i.e., an expanded version of Fig. 1. A summary of the computational steps is also given in Appendix F. In Appendix G, we provide a convergence guarantee for the ADMM (34). In Appendix I, we comment on different ways to implement the proposed algorithm depending on the number of ways to group the summand functionals in (1).

5 Experiments

We report two numerical experiments to illustrate the proposed framework. All simulations are performed on a MacBook Air with 1.1 GHz Intel Core i5 CPU with 8 GB RAM.

Linear Fokker-Planck a.k.a. Kolmogorov's forward PDE. We consider computing the solution $\mu(\boldsymbol{\theta}, t)$ for the IVP $\frac{\partial \mu}{\partial t} = \nabla \cdot (\mu \nabla V) + \beta^{-1} \Delta \mu$, $\mu(\boldsymbol{\theta}, t = 0) = \mu_0(\boldsymbol{\theta})$ (given) where $\boldsymbol{\theta} \equiv (\theta_1, \theta_2) \in \mathbb{R}^2$ with $V(\theta_1, \theta_2) = \frac{1}{4}(1 + \theta_1^4) + \frac{1}{2}(\theta_2^2 - \theta_1^2)$, $\beta > 0$. The stationary measure $\mu_\infty \propto \exp(-\beta V) d\boldsymbol{\theta}$, which for our choice of V , is bimodal.

For distributed computation, here $n = 2$ and following Table 1, we choose $F_1(\boldsymbol{\mu}_1) = \langle \mathbf{V}_k, \boldsymbol{\mu}_1 \rangle$, $F_2(\boldsymbol{\mu}_2) = \langle \beta^{-1} \log \boldsymbol{\mu}_2, \boldsymbol{\mu}_2 \rangle$. The drift potential $\mathbf{V}_k(j) := V(\boldsymbol{\theta}_k^j)$ for sample index $j \in [N]$. Since F_1 is linear in $\boldsymbol{\mu}_1$, we use (35) with $\Phi_1(\boldsymbol{\mu}_1) = \langle \mathbf{V}_{k-1} + \boldsymbol{\nu}_1^k, \boldsymbol{\mu}_1 \rangle$ to analytically compute the proximal updates $\boldsymbol{\mu}_1^{k+1}$, $k \in \mathbb{N}_0$. The simulation parameters are $\alpha = 12$, $\tau = 150$, $\beta = 1$, and $\varepsilon = 5 \times 10^{-2}$. To compute the proximal updates $\boldsymbol{\mu}_2^{k+1}$ via (27), we use the PROXRECUR algorithm from Caluya & Halder (2019, Sec. III-B.1) with algorithmic parameters $\delta = 10^{-4}$, $L = 20$. For doing so, we generate $N = 1681$ uniform grid samples over $[-2, 2]^2$, and use the initial distribution (five component mixture of Gaussians) $\boldsymbol{\mu}_0 = \frac{1}{5} \sum_{i=1}^5 \mathcal{N}(\mathbf{m}_i, \boldsymbol{\Sigma})$ with $\mathbf{m}_1 = (1, 1)^\top$, $\mathbf{m}_2 = (-1, -1)^\top$, $\mathbf{m}_3 = (1, -1)^\top$, $\mathbf{m}_4 = (-1, 1)^\top$, $\mathbf{m}_5 = (0, 0)^\top$, $\boldsymbol{\Sigma} = 0.1 \mathbf{I}_2$.

The resulting evolution of $\boldsymbol{\mu}_1$ and $\boldsymbol{\mu}_2$ are shown in Fig. 2. After 5000 iterations of the outer layer ADMM (23), both $\boldsymbol{\mu}_1$ and $\boldsymbol{\mu}_2$ tend to the known μ_∞ . We performed only 3 iterations for the inner layer ADMM (34). The total simulation time was 99.89 sec.

Aggregation-drift-diffusion nonlinear PDE. We next consider solving a nonlinear PDE IVP $\frac{\partial \mu}{\partial t} = \nabla \cdot (\mu \nabla (U \circledast \mu)) + \nabla \cdot (\mu \nabla V) + \beta^{-1} \Delta \mu^2$ with $\boldsymbol{\theta} \in \mathbb{R}^2$, the same μ_0 as in the previous

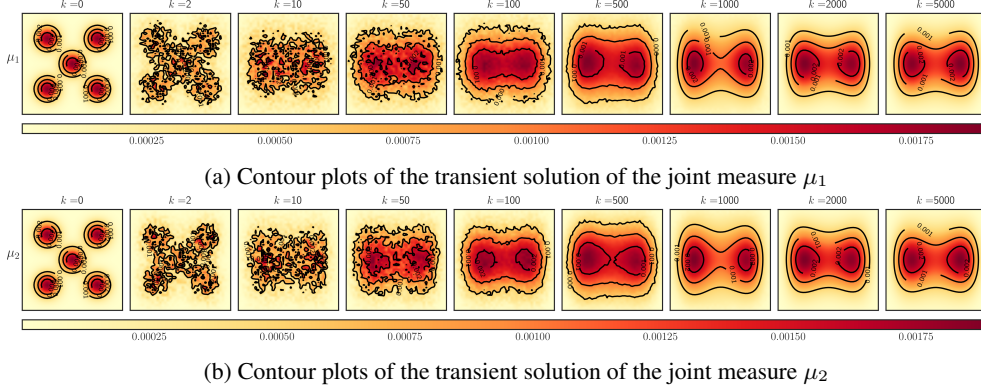


Figure 2: Distributed computation for solving the linear Fokker–Planck IVP over domain $[-2, 2]^2$. Color denotes the value of the plotted variable; see colorbar (dark red = high, light yellow = low).

example, $U(\boldsymbol{\theta}) = \frac{1}{2} \|\boldsymbol{\theta}\|_2^2 - \ln \|\boldsymbol{\theta}\|_2$, and $V(\boldsymbol{\theta}) = -\frac{1}{4} \ln \|\boldsymbol{\theta}\|_2$. As $\beta^{-1} \downarrow 0$, the stationary solution μ_∞ is a uniform measure over annulus (Carrillo et al., 2022, Sec. 4.3.2) with the inner and outer radii of $R_i = 1/2$ and $R_o = \sqrt{5}/2$, respectively. To avoid evaluation of U and V at $\boldsymbol{\theta} = \mathbf{0}$, we set $U(\mathbf{0})$ and $V(\mathbf{0})$ to be equal to the respective average values of U and V on the cell of width $2h$ centered at $(0, 0)$. In our simulation, $h = 5 \times 10^{-3}$.

Here, we have three spatial operators: interaction $\nabla \cdot (\mu \nabla (U \circledast \mu))$, drift $\nabla \cdot (\mu \nabla V)$, and diffusion $\beta^{-1} \Delta \mu^2$. In Appendix H, we detail four different ways of splitting the operators and present quantitative results for each case. For the splitting $F_1(\mu_1) = \langle \mathbf{V}_k + \beta^{-1} \log \mu_1, \mu_1 \rangle$, $F_2(\mu_2) = \langle \mathbf{U}_k \mu_2^k, \mu_2 \rangle$, the evolution of μ_1 and μ_2 are shown in Fig. 3 which match with each other and with the annulus mentioned before. Appendix H provides more details on this numerical experiment.

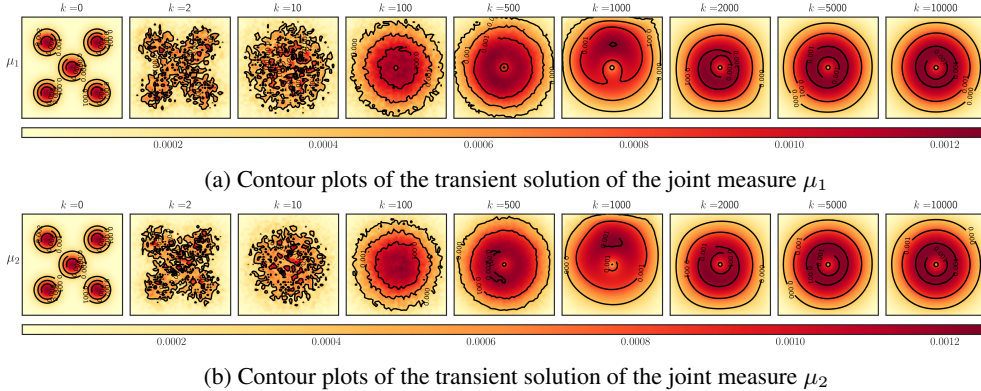


Figure 3: Distributed computation for solving the nonlinear aggregation-drift-diffusion IVP over domain $[-2, 2]^2$ for $F_1(\mu_1) = \langle \mathbf{V}_k + \beta^{-1} \log \mu_1, \mu_1 \rangle$, $F_2(\mu_2) = \langle \mathbf{U}_k \mu_2^k, \mu_2 \rangle$. Color denotes the value of the plotted variable; see colorbar (dark red = high, light yellow = low).

6 Conclusions

We present a novel computational framework to solve measure-valued optimization problems with additive objective via distributed computation. Our findings provide new insights in generalizing the well-known finite dimensional Euclidean ADMM to its Wasserstein and Sinkhorn counterparts, and open up the possibility of designing measure-valued operator splitting algorithms. The proposed framework leverages existing proximal and Jordan-Kinderlehrer-Otto (JKO) schemes. Its feasibility is demonstrated via illustrative numerical experiments. While we provided convergence guarantee (Appendix G) for the proposed inner layer ADMM, an important undertaking not pursued here is the convergence guarantee for the overall scheme. This will be the topic of our future work.

References

- Martial Agueh and Guillaume Carlier. Barycenters in the wasserstein space. *SIAM Journal on Mathematical Analysis*, 43(2):904–924, 2011.
- David Alvarez-Melis, Yair Schiff, and Youssef Mroueh. Optimizing functionals on the space of probabilities with input convex neural networks. *arXiv preprint arXiv:2106.00774*, 2021.
- Luigi Ambrosio, Nicola Gigli, and Giuseppe Savaré. *Gradient flows: in metric spaces and in the space of probability measures*. Springer Science & Business Media, 2008.
- Ferran Arqué, César A Uribe, and Carlos Ocampo-Martinez. Approximate Wasserstein attraction flows for dynamic mass transport over networks. *Automatica*, 143:110432, 2022.
- HH Bauschke and SG Kruk. Reflection-projection method for convex feasibility problems with an obtuse cone. *Journal of Optimization Theory and Applications*, 120(3):503–531, 2004.
- Eric Temple Bell. The iterated exponential integers. *Annals of Mathematics*, pp. 539–557, 1938.
- Jean-David Benamou, Guillaume Carlier, Marco Cuturi, Luca Nenna, and Gabriel Peyré. Iterative Bregman projections for regularized transportation problems. *SIAM Journal on Scientific Computing*, 37(2):A1111–A1138, 2015.
- Jean-David Benamou, Guillaume Carlier, and Maxime Laborde. An augmented Lagrangian approach to Wasserstein gradient flows and applications. *ESAIM: Proceedings and surveys*, 54:1–17, 2016.
- Espen Bernton. Langevin monte carlo and JKO splitting. In *Conference on learning theory*, pp. 1777–1798. PMLR, 2018.
- Malcolm Bowles and Martial Agueh. Weak solutions to a fractional Fokker–Planck equation via splitting and Wasserstein gradient flow. *Applied Mathematics Letters*, 42:30–35, 2015.
- Stephen Boyd, Stephen P Boyd, and Lieven Vandenbergh. *Convex optimization*. Cambridge university press, 2004.
- Stephen Boyd, Neal Parikh, and Eric Chu. *Distributed optimization and statistical learning via the alternating direction method of multipliers*. Now Publishers Inc, 2011.
- Yann Brenier. Polar factorization and monotone rearrangement of vector-valued functions. *Communications on pure and applied mathematics*, 44(4):375–417, 1991.
- Charlotte Bunne, Laetitia Papaxanthos, Andreas Krause, and Marco Cuturi. Proximal optimal transport modeling of population dynamics. In *International Conference on Artificial Intelligence and Statistics*, pp. 6511–6528. PMLR, 2022.
- Dan Butnariu and Alfredo N Iusem. *Totally convex functions for fixed points computation and infinite dimensional optimization*, volume 40. Springer Science & Business Media, 2000.
- Kenneth Caluya and Abhishek Halder. Wasserstein proximal algorithms for the Schrödinger bridge problem: Density control with nonlinear drift. *IEEE Transactions on Automatic Control*, 2021.
- Kenneth F Caluya and Abhishek Halder. Gradient flow algorithms for density propagation in stochastic systems. *IEEE Transactions on Automatic Control*, 65(10):3991–4004, 2019.
- Guillaume Carlier, Vincent Duval, Gabriel Peyré, and Bernhard Schmitzer. Convergence of entropic schemes for optimal transport and gradient flows. *SIAM Journal on Mathematical Analysis*, 49(2): 1385–1418, 2017.
- José A Carrillo, Katy Craig, Li Wang, and Chaozhen Wei. Primal dual methods for Wasserstein gradient flows. *Foundations of Computational Mathematics*, 22(2):389–443, 2022.
- Lenaic Chizat and Francis Bach. On the global convergence of gradient descent for over-parameterized models using optimal transport. *Advances in neural information processing systems*, 31, 2018.

- Casey Chu, Jose Blanchet, and Peter Glynn. Probability functional descent: A unifying perspective on GANs, variational inference, and reinforcement learning. In *International Conference on Machine Learning*, pp. 1213–1222. PMLR, 2019.
- Marco Cuturi. Sinkhorn distances: Lightspeed computation of optimal transport. *Advances in neural information processing systems*, 26:2292–2300, 2013.
- Marco Cuturi and Gabriel Peyré. A smoothed dual approach for variational Wasserstein problems. *SIAM Journal on Imaging Sciences*, 9(1):320–343, 2016.
- Carles Domingo-Enrich, S Jelassi, A Mensch, G Rotskoff, and J Bruna. A mean-field analysis of two-player zero-sum games. *Advances in neural information processing systems*, 2020.
- Pavel Dvurechenskii, Darina Dvinskikh, Alexander Gasnikov, Cesar Uribe, and Angelia Nedich. Decentralize and randomize: Faster algorithm for Wasserstein barycenters. *Advances in Neural Information Processing Systems*, 31, 2018.
- Jiaojiao Fan, Qinsheng Zhang, Amirhossein Taghvaei, and Yongxin Chen. Variational Wasserstein gradient flow. In *International Conference on Machine Learning*, pp. 6185–6215. PMLR, 2022.
- Charlie Frogner and Tomaso Poggio. Approximate inference with Wasserstein gradient flows. In *International Conference on Artificial Intelligence and Statistics*, pp. 2581–2590. PMLR, 2020.
- Daniel Gabay and Bertrand Mercier. A dual algorithm for the solution of nonlinear variational problems via finite element approximation. *Computers & mathematics with applications*, 2(1): 17–40, 1976.
- Thomas O Gallouët and Leonard Monsaingeon. A JKO splitting scheme for Kantorovich–Fisher–Rao gradient flows. *SIAM Journal on Mathematical Analysis*, 49(2):1100–1130, 2017.
- Aude Genevay, Marco Cuturi, Gabriel Peyré, and Francis Bach. Stochastic optimization for large-scale optimal transport. In *NIPS 2016-Thirtieth Annual Conference on Neural Information Processing System*, pp. 3440–3448, 2016.
- Roland Glowinski and Patrick Le Tallec. *Augmented Lagrangian and operator-splitting methods in nonlinear mechanics*. SIAM, 1989.
- Roland Glowinski, Tsorng-Whay Pan, and Xue-Cheng Tai. Some facts about operator-splitting and alternating direction methods. *Splitting Methods in Communication, Imaging, Science, and Engineering*, pp. 19–94, 2016.
- RL Graham, DE Knuth, and O Patashnik. *Concrete mathematics*, 1988.
- Mingyi Hong, Zhi-Quan Luo, and Meisam Razaviyayn. Convergence analysis of alternating direction method of multipliers for a family of nonconvex problems. *SIAM Journal on Optimization*, 26(1): 337–364, 2016.
- Kazufumi Ito and Karl Kunisch. The augmented Lagrangian method for equality and inequality constraints in Hilbert spaces. *Mathematical programming*, 46(1-3):341–360, 1990.
- Richard Jordan, David Kinderlehrer, and Felix Otto. The variational formulation of the Fokker–Planck equation. *SIAM journal on mathematical analysis*, 29(1):1–17, 1998.
- Christian Kanzow, Daniel Steck, and Daniel Wachsmuth. An augmented Lagrangian method for optimization problems in Banach spaces. *SIAM Journal on Control and Optimization*, 56(1): 272–291, 2018.
- Johan Karlsson and Axel Ringh. Generalized Sinkhorn iterations for regularizing inverse problems using optimal mass transport. *SIAM Journal on Imaging Sciences*, 10(4):1935–1962, 2017.
- Carson Kent, Jiajin Li, Jose Blanchet, and Peter W Glynn. Modified Frank Wolfe in probability space. *Advances in Neural Information Processing Systems*, 34:14448–14462, 2021.

- Maxime Laborde. On some nonlinear evolution systems which are perturbations of Wasserstein gradient flows. *Topological Optimization and Optimal Transport: In the Applied Sciences*, 17:304, 2017.
- Bas Lemmens and Roger Nussbaum. *Nonlinear Perron-Frobenius Theory*, volume 189. Cambridge University Press, 2012.
- Song Mei, Andrea Montanari, and Phan-Minh Nguyen. A mean field view of the landscape of two-layer neural networks. *Proceedings of the National Academy of Sciences*, 115(33):E7665–E7671, 2018.
- Petr Mokrov, Alexander Korotin, Lingxiao Li, Aude Genevay, Justin M Solomon, and Evgeny Burnaev. Large-scale Wasserstein gradient flows. *Advances in Neural Information Processing Systems*, 34:15243–15256, 2021.
- Yurii Nesterov. *Introductory lectures on convex optimization: A basic course*, volume 87. Springer Science and Business Media, 2003.
- Robert Nishihara, Laurent Lessard, Ben Recht, Andrew Packard, and Michael Jordan. A general analysis of the convergence of ADMM. In *International Conference on Machine Learning*, pp. 343–352. PMLR, 2015.
- Neal Parikh and Stephen Boyd. Proximal algorithms. *Foundations and Trends in optimization*, 1(3): 127–239, 2014.
- Gabriel Peyré. Entropic approximation of Wasserstein gradient flows. *SIAM Journal on Imaging Sciences*, 8(4):2323–2351, 2015.
- Adil Salim, Anna Korba, and Giulia Luise. The Wasserstein proximal gradient algorithm. *Advances in Neural Information Processing Systems*, 33:12356–12366, 2020.
- Filippo Santambrogio. {Euclidean, metric, and Wasserstein} gradient flows: an overview. *Bulletin of Mathematical Sciences*, 7(1):87–154, 2017.
- Justin Sirignano and Konstantinos Spiliopoulos. Mean field analysis of neural networks: A central limit theorem. *Stochastic Processes and their Applications*, 130(3):1820–1852, 2020.
- Anthony C Thompson. On certain contraction mappings in a partially ordered vector space. *Proceedings of the American Mathematical Society*, 14(3):438–443, 1963.
- Cédric Villani. *Topics in optimal transportation*, volume 58. American Mathematical Soc., 1st edition, 2003.
- Cédric Villani. *Optimal transport: old and new*, volume 338. Springer, 2009.
- Yifei Wang and Wuchen Li. Accelerated information gradient flow. *Journal of Scientific Computing*, 90:1–47, 2022.
- Yu Wang, Wotao Yin, and Jinshan Zeng. Global convergence of ADMM in nonconvex nonsmooth optimization. *Journal of Scientific Computing*, 78(1):29–63, 2019.
- Andre Wibisono. Sampling as optimization in the space of measures: The Langevin dynamics as a composite optimization problem. In *Conference on Learning Theory*, pp. 2093–3027. PMLR, 2018.
- Lei Yang, Jia Li, Defeng Sun, and Kim-Chuan Toh. A fast globally linearly convergent algorithm for the computation of Wasserstein barycenters. *The Journal of Machine Learning Research*, 22(1): 984–1020, 2021.
- Ruiyi Zhang, Changyou Chen, Chunyuan Li, and Lawrence Carin. Policy optimization as Wasserstein gradient flows. In *International Conference on Machine Learning*, pp. 5737–5746. PMLR, 2018.

A Examples of F_i and Wasserstein Gradient Flows

In this Section, we provide specific examples of F_i, Φ_i in (20), and the associated Wasserstein gradient flows (WGFs) (21).

We denote the base space as $\mathcal{X} \subseteq \mathbb{R}^d$ and its element as $\theta \in \mathcal{X}$. For fixed $i \in [n]$, important examples of F_i include $\int_{\mathcal{X}} V(\theta) d\mu_i(\theta)$ (potential energy for some suitable advection potential V), $\beta^{-1} \int_{\mathcal{X}} \log \mu_i(\theta) d\mu_i(\theta)$ (logarithmic internal energy with the ‘‘inverse temperature’’ parameter $\beta > 0$), $\int_{\mathcal{X} \times \mathcal{X}} U(\theta, \sigma) d\mu_i(\theta) d\mu_i(\sigma)$ (interaction energy for some symmetric positive definite interaction potential U), and $(\beta^{-1}/(m-1)) \int_{\mathcal{X}} \mu_i^{m-1}(\theta) d\mu_i(\theta)$ (power law internal energy).

In Table 1, we summarize how the WGF (21) specializes in such cases. In particular, the PDEs in the second column of Table 1 are well known: the Liouville advection PDE (first row), the Fokker-Planck a.k.a. Kolmogorov’s forward advection-diffusion PDE (second row), the advection-aggregation a.k.a. propagation of chaos PDE (third row), and the porous medium a.k.a. advection-nonlinear power law diffusion PDE (fourth row).

$\Phi_i(\cdot) = F_i(\cdot) + \int \nu_i^k d(\cdot)$	WGF (21)
$\int_{\mathcal{X}} (V(\theta) + \nu_i^k(\theta)) d\mu_i(\theta)$	$\frac{\partial \tilde{\mu}_i}{\partial t} = \nabla \cdot (\tilde{\mu}_i (\nabla V + \nabla \nu_i^k))$
$\int_{\mathcal{X}} (\nu_i^k(\theta) + \beta^{-1} \log \mu_i(\theta)) d\mu_i(\theta)$	$\frac{\partial \tilde{\mu}_i}{\partial t} = \nabla \cdot (\tilde{\mu}_i \nabla \nu_i^k) + \beta^{-1} \Delta \tilde{\mu}_i$
$\int_{\mathcal{X}} \nu_i^k(\theta) d\mu_i(\theta) + \int_{\mathcal{X} \times \mathcal{X}} U(\theta, \sigma) d\mu_i(\theta) d\mu_i(\sigma)$	$\frac{\partial \tilde{\mu}_i}{\partial t} = \nabla \cdot (\tilde{\mu}_i (\nabla \nu_i^k + \nabla (U \circledast \tilde{\mu}_i)))$
$\int_{\mathcal{X}} (\nu_i^k(\theta) + \frac{\beta^{-1}}{m-1} \mu_i^{m-1}) d\mu_i(\theta), m > 1$	$\frac{\partial \tilde{\mu}_i}{\partial t} = \nabla \cdot (\tilde{\mu}_i \nabla \nu_i^k) + \beta^{-1} \Delta \tilde{\mu}_i^m$

Table 1: Specific instances of the WGF (21) for different choices of F_i , and hence Φ_i . The Euclidean gradient operator ∇ is w.r.t. $\theta \in \mathcal{X}$. The operator \circledast can be seen as a generalized convolution, given by $(U \circledast \tilde{\mu}_i)(\theta) := \int_{\mathcal{X}} U(\theta, \sigma) d\tilde{\mu}_i(\sigma)$ where $U(\theta, \sigma)$ is symmetric and positive definite for all $(\theta, \sigma) \in \mathcal{X} \times \mathcal{X} \subseteq \mathbb{R}^d \times \mathbb{R}^d$.

We emphasize here that different from standard WGF literature, the functionals $\Phi_i(\cdot)$ listed in Table 1 are a sum of two functionals: a ‘‘physical’’ free energy functional $F_i(\cdot)$ (e.g., advection, diffusion, interaction), and an ‘‘algorithmic’’ linear functional $\int \nu_i^k d(\cdot)$ that specifically arises from our consensus constraint. The latter is an algorithmic construct and has no physical meaning.

B Examples of μ Updates

In this Section, we exemplify the usage of Proposition 1 for several functionals of practical interest.

Example: $F_i(\mu_i) = \beta^{-1} \langle \log \mu_i, \mu_i \rangle, \beta > 0$.

As pointed out in Table 1 second row, this specific choice of F_i correspond to WGF with advection and linear diffusion. In this case, Proposition 1 reduces exactly to (Caluya & Halder, 2019, Theorem 1) allowing further simplification of (26b). In particular, the system (26) can be solved via certain cone-preserving block coordinate iteration proposed in (Caluya & Halder, 2019, Sec. III.B,C) that is *provably contractive w.r.t. the Thompson metric* (Thompson, 1963) (Lemmens & Nussbaum, 2012, Ch. 2.1). Consequently, the block coordinate iteration is guaranteed to converge to a unique pair $(\lambda_{0i}^{\text{opt}}, \lambda_{1i}^{\text{opt}})$ with linear rate of convergence. This makes the proximal update (27) semi-analytical in the sense the pair $(\lambda_{0i}^{\text{opt}}, \lambda_{1i}^{\text{opt}})$ can be numerically computed by performing the contractive block coordinate iteration while ‘‘freezing’’ the index $k \in \mathbb{N}_0$. With the converged pair $(\lambda_{0i}^{\text{opt}}, \lambda_{1i}^{\text{opt}})$, the evaluation (27) is analytical for each $k \in \mathbb{N}_0$.

Example: $F_i(\mu_i) = \langle \mathbf{V}, \mu_i \rangle$.

When F_i and hence G_i in (24), is linear in μ_i , the proximal update μ_i^{k+1} can be computed analytically, obviating the zero order hold sub-iterations mentioned in the previous example. We summarize this novel result in the following Theorem 2. Notice in particular that the case of advection PDE shown in the first row of Table 1 can be treated via Theorem 2 with $\Phi_i(\mu_i) = \langle \mathbf{V} + \nu_i^k, \mu_i \rangle$, for given $i \in [n]$.

In this discrete version, $\mathbf{V} \in \mathbb{R}^N$ is the advection potential evaluated at the N sample locations in \mathbb{R}^d .

Theorem 2. Given $\mathbf{a} \in \mathbb{R}^N \setminus \{\mathbf{0}\}$, let $\Phi(\boldsymbol{\mu}) := \langle \mathbf{a}, \boldsymbol{\mu} \rangle$ for $\boldsymbol{\mu} \in \Delta^{N-1}$. Let $\mathbf{C} \in \mathbb{R}^{N \times N}$ be the squared Euclidean distance matrix, and for $\varepsilon > 0$, let $\boldsymbol{\Gamma} := \exp(-\mathbf{C}/2\varepsilon)$. For any $\boldsymbol{\zeta} \in \Delta^{N-1}$, $\alpha > 0$, the proximal operator

$$\text{prox}_{\frac{1}{\alpha}\Phi}^{W_\varepsilon}(\boldsymbol{\zeta}) = \exp\left(-\frac{1}{\alpha\varepsilon}\mathbf{a}\right) \odot \left(\boldsymbol{\Gamma}^\top \left(\boldsymbol{\zeta} \odot \left(\boldsymbol{\Gamma} \exp\left(-\frac{1}{\alpha\varepsilon}\mathbf{a}\right)\right)\right)\right). \quad (35)$$

Proof. We start from (25) by dropping the indices i and k , and set $G(\boldsymbol{\mu}) = \langle \mathbf{a}, \boldsymbol{\mu} \rangle$, where $\mathbf{a} \in \mathbb{R}^N \setminus \{\mathbf{0}\}$.

For notational ease, let $\mathbf{y} := \exp\left(\frac{\lambda_0}{\alpha\varepsilon}\right) \in \mathbb{R}_{>0}^N$, $\mathbf{z} := \exp\left(\frac{\lambda_1}{\alpha\varepsilon}\right) \in \mathbb{R}_{>0}^N$. Since G is linear, its Legendre-Fenchel conjugate is an indicator function:

$$G^*(-\lambda_1) = \begin{cases} 0 & \text{if } \lambda_1 = -\mathbf{a}, \\ +\infty & \text{otherwise.} \end{cases}$$

Therefore, (25) yields

$$\lambda_0^{\text{opt}} = \arg \max_{\lambda_0 \in \mathbb{R}^N} \left\{ \langle \lambda_0, \boldsymbol{\zeta} \rangle - \alpha\varepsilon \langle \mathbf{y}, \boldsymbol{\Gamma} \mathbf{z} \rangle \right\}, \quad (36a)$$

$$\lambda_1^{\text{opt}} = -\mathbf{a}. \quad (36b)$$

From (36b),

$$\mathbf{z}^{\text{opt}} = \exp\left(-\frac{1}{\alpha\varepsilon}\mathbf{a}\right). \quad (37)$$

Setting the gradient of the objective in (36a) to zero, determines λ_0^{opt} , or equivalently \mathbf{y}^{opt} as

$$\mathbf{y}^{\text{opt}} = \boldsymbol{\zeta} \odot (\boldsymbol{\Gamma} \mathbf{z}^{\text{opt}}). \quad (38)$$

From (27), the proximal update is

$$\begin{aligned} \text{prox}_{\frac{1}{\alpha}\Phi}^{W_\varepsilon}(\boldsymbol{\zeta}) &= \mathbf{z}^{\text{opt}} \odot (\boldsymbol{\Gamma}^\top \mathbf{y}^{\text{opt}}) \\ &\stackrel{(38)}{=} \mathbf{z}^{\text{opt}} \odot (\boldsymbol{\Gamma}^\top (\boldsymbol{\zeta} \odot (\boldsymbol{\Gamma} \mathbf{z}^{\text{opt}}))). \end{aligned} \quad (39)$$

Substituting (37) in (39), we arrive at (35). ■

Example: $F_i(\boldsymbol{\mu}_i) = \langle \mathbf{U} \boldsymbol{\mu}_i, \boldsymbol{\mu}_i \rangle$.

The case of advection-aggregation PDE shown in the third row of Table 1 leads to $F_i(\boldsymbol{\mu}_i) = \langle \mathbf{U} \boldsymbol{\mu}_i, \boldsymbol{\mu}_i \rangle$, and thus $\Phi_i(\boldsymbol{\mu}_i) = \langle \mathbf{U} \boldsymbol{\mu}_i + \boldsymbol{\nu}_i^k, \boldsymbol{\mu}_i \rangle$ for given $i \in [n]$. In this discrete version, $\mathbf{U} \in \mathbb{R}^{N \times N}$ is the interaction potential. Following Benamou et al. (2016, Sec. 4), we approximate $\Phi_i(\boldsymbol{\mu}_i) \approx \widehat{\Phi}_i(\boldsymbol{\mu}_i, \boldsymbol{\mu}_i^k) := \langle \mathbf{U} \boldsymbol{\mu}_i^k + \boldsymbol{\nu}_i^k, \boldsymbol{\mu}_i \rangle$, resulting in semi-implicit variant of the proximal update (23a) given by

$$\boldsymbol{\mu}_i^{k+1} = \text{prox}_{\frac{1}{\alpha}\widehat{\Phi}_i(\boldsymbol{\mu}_i, \boldsymbol{\mu}_i^k)}^{W_\varepsilon}(\boldsymbol{\zeta}^k) = \text{prox}_{\frac{1}{\alpha}(\langle \mathbf{U} \boldsymbol{\mu}_i^k + \boldsymbol{\nu}_i^k, \boldsymbol{\mu}_i \rangle)}^{W_\varepsilon}(\boldsymbol{\zeta}^k), \quad k \in \mathbb{N}_0.$$

Convergence and consistency guarantees for such semi-implicit scheme are available, see e.g., (Laborde, 2017, Sec. 12.3). Such semi-implicit schemes allow us to apply Theorem 2 by setting $\widehat{\Phi}_i(\boldsymbol{\mu}_i) \equiv \widehat{\Phi}_i(\boldsymbol{\mu}_i, \boldsymbol{\mu}_i^k)$, for given $i \in [n]$.

Example: $F_i(\boldsymbol{\mu}_i) = \langle \frac{\beta^{-1}}{m-1} \mathbf{1}, \boldsymbol{\mu}_i^m \rangle = \frac{\beta^{-1}}{m-1} \|\boldsymbol{\mu}_i\|_m^m$, $m > 1$.

The case of porous medium a.k.a. advection-nonlinear power law diffusion PDE shown in the fourth row of Table 1 corresponds to $F_i(\boldsymbol{\mu}_i) = \langle \frac{\beta^{-1}}{m-1} \mathbf{1}, \boldsymbol{\mu}_i^m \rangle$ (vector exponent m is elementwise), and thus $\Phi_i(\boldsymbol{\mu}_i) = \langle \frac{\beta^{-1}}{m-1} \boldsymbol{\mu}_i^{m-1} + \boldsymbol{\nu}_i^k, \boldsymbol{\mu}_i \rangle$ for given $i \in [n]$. In this case, the proximal update becomes amenable via the following result.

Theorem 3. Given $\boldsymbol{\nu}^k \in \mathbb{R}^N$, $\beta > 0$, $m > 1$, let $\Phi(\boldsymbol{\mu}) := \langle \frac{\beta^{-1}}{m-1} \boldsymbol{\mu}^{m-1} + \boldsymbol{\nu}^k, \boldsymbol{\mu} \rangle$ for $\boldsymbol{\mu} \in \Delta^{N-1}$.

Let $\mathbf{C} \in \mathbb{R}^{N \times N}$ be the squared Euclidean distance matrix, and for $\varepsilon > 0$, let $\boldsymbol{\Gamma} := \exp(-\mathbf{C}/2\varepsilon)$. For any $\boldsymbol{\zeta} \in \Delta^{N-1}$, $\alpha > 0$, let $(\mathbf{y}^{\text{opt}}, \mathbf{z}^{\text{opt}}) \in \mathbb{R}_{>0}^N \times \mathbb{R}_{>0}^N$ be the solution of

$$\mathbf{y} \odot (\boldsymbol{\Gamma}^\top \mathbf{z}) = \boldsymbol{\zeta}, \quad (40a)$$

$$\begin{aligned} \mathbf{z} \odot (\boldsymbol{\Gamma}^\top \mathbf{y}) &= (\beta)^{\frac{1}{m-1}} \left(\frac{m-1}{m} \right)^{\frac{m}{m-1}} \left(-\frac{m}{m-1} \right) \\ &\quad \left(\mathbf{1}^\top (-\alpha\varepsilon \ln(\mathbf{z}) - \boldsymbol{\nu}^k)^m \right)^{\frac{2-m}{m-1}} (-\alpha\varepsilon \ln(\mathbf{z}) - \boldsymbol{\nu}^k)^{m-1}. \end{aligned} \quad (40b)$$

Then

$$\text{prox}_{\frac{1}{\alpha}\Phi}^{W_\varepsilon}(\boldsymbol{\zeta}) = \mathbf{z}^{\text{opt}} \odot (\boldsymbol{\Gamma}^\top \mathbf{y}^{\text{opt}}). \quad (41)$$

Proof. The Legendre-Fenchel conjugate of $\Phi(\boldsymbol{\mu})$ is

$$\Phi^*(\boldsymbol{\lambda}) = \sup_{\boldsymbol{\mu}} \left\{ \boldsymbol{\lambda}^\top \boldsymbol{\mu} - (\boldsymbol{\nu}^k)^\top \boldsymbol{\mu} - \frac{\beta^{-1}}{m-1} \mathbf{1}^\top \boldsymbol{\mu}_i^m \right\}. \quad (42)$$

From (42), direct computation gives

$$\Phi^*(\boldsymbol{\lambda}) = \left(\beta \left(\frac{m-1}{m} \mathbf{1}^\top (\boldsymbol{\lambda} - \boldsymbol{\nu}^k) \right)^m \right)^{\frac{1}{m-1}}. \quad (43)$$

Let $\mathbf{y} := \exp\left(\frac{\boldsymbol{\lambda}_0}{\alpha\varepsilon}\right) \in \mathbb{R}_{>0}^N$, $\mathbf{z} := \exp\left(\frac{\boldsymbol{\lambda}_1}{\alpha\varepsilon}\right) \in \mathbb{R}_{>0}^N$, and drop the subscripts i in (25) for notational ease. Fixing $\boldsymbol{\lambda}_1$, and taking the gradient of the objective in (25) w.r.t. $\boldsymbol{\lambda}_0$ gives (40a).

On the other hand, fixing $\boldsymbol{\lambda}_0$, and taking the gradient of the objective in (25) w.r.t. $\boldsymbol{\lambda}_1$ gives

$$\nabla_{\boldsymbol{\lambda}_1} \Phi^*(-\boldsymbol{\lambda}_1) = \mathbf{z} \odot (\boldsymbol{\Gamma}^\top \mathbf{y}). \quad (44)$$

Using (43) into the left hand side of (44) results in (40b). Finally, (27) yields the proximal update (41). \blacksquare

Remark 4. That the unique pair $(\mathbf{y}^{\text{opt}}, \mathbf{z}^{\text{opt}}) \in \mathbb{R}_{>0}^N \times \mathbb{R}_{>0}^N$ can be found from cone-preserving contractive fixed point recursion, follows from nonlinear Perron-Frobenius theory as in (Caluya & Halder, 2019, Sec. III-C). In Sec. 5, we provide numerical results for advection-nonlinear power law diffusion with $m = 2$.

C Proof of Theorem 1

We make use of the following Proposition from Cuturi & Peyré (2016, Sec. 4.1), rephrased in our notation.

Proposition 2. (Cuturi & Peyré, 2016, Proposition 1) Let

$$W_{\varepsilon, \boldsymbol{\mu}_i}^2(\boldsymbol{\zeta}) := \min_{\mathbf{M}_i \in \Pi_N(\boldsymbol{\mu}_i, \boldsymbol{\zeta})} \left\langle \frac{1}{2} \mathbf{C} + \varepsilon \log \mathbf{M}_i, \mathbf{M}_i \right\rangle, \quad \varepsilon > 0,$$

for given $\boldsymbol{\mu}_i \in \Delta^{N-1}$ for all $i \in [n]$, and for a given squared Euclidean distance matrix $\mathbf{C} \in \mathbb{R}^{N \times N}$. Let the superscript $*$ denote the Legendre-Fenchel conjugate. Given weights $w_1, \dots, w_n > 0$, linear operator \mathcal{A} , and a convex real-valued function J , consider the variational problem

$$\boldsymbol{\zeta}^{\text{opt}} = \arg \min_{\boldsymbol{\zeta} \in \Delta^{N-1}} \sum_{i=1}^n w_i W_{\varepsilon, \boldsymbol{\mu}_i}^2(\boldsymbol{\zeta}) + J(\mathcal{A}\boldsymbol{\zeta}). \quad (45)$$

The dual problem of (45) is given by

$$\begin{aligned} (\mathbf{u}_1^{\text{opt}}, \dots, \mathbf{u}_n^{\text{opt}}, \mathbf{v}^{\text{opt}}) &= \arg \min_{(\mathbf{u}_1, \dots, \mathbf{u}_n, \mathbf{v}) \in \mathbb{R}^{(n+1)N}} \sum_{i=1}^n w_i (W_{\varepsilon, \boldsymbol{\mu}_i}^2)^*(\mathbf{u}_i) + J^*(\mathbf{v}) \\ &\text{subject to } \mathcal{A}^* \mathbf{v} + \sum_{i=1}^n w_i \mathbf{u}_i = \mathbf{0}, \end{aligned} \quad (46)$$

and the primal-dual relation giving the minimizer in (45) is

$$\boldsymbol{\zeta}^{\text{opt}} = \nabla_{\mathbf{u}_i} (W_{\varepsilon, \boldsymbol{\mu}_i}^2)^*(\mathbf{u}_i^{\text{opt}}) \in \Delta^{N-1}, \quad \text{for all } i \in [n]. \quad (47)$$

We recast (23b) in the form (45) by setting the probability vectors $\boldsymbol{\mu}_i \equiv \boldsymbol{\mu}_i^{k+1}$, the weights $w_1 = w_2 = \dots = w_n = 1$, the operator \mathcal{A} as identity, and the function $J(\cdot) \equiv \langle -\frac{2}{\alpha} \boldsymbol{\nu}_{\text{sum}}^k, \cdot \rangle$. Since J is linear, we have

$$J^*(\mathbf{v}) = \begin{cases} 0 & \text{if } \mathbf{v} = -\frac{2}{\alpha} \boldsymbol{\nu}_{\text{sum}}^k, \\ +\infty & \text{otherwise.} \end{cases} \quad (48)$$

Also, \mathcal{A} being the identity operator, we get $\mathcal{A}^* \mathbf{v} = \mathbf{v}$. Therefore, the dual problem (46) corresponding to (23b) becomes

$$\begin{aligned} (\mathbf{u}_1^{\text{opt}}, \dots, \mathbf{u}_n^{\text{opt}}) &= \arg \min_{(\mathbf{u}_1, \dots, \mathbf{u}_n) \in \mathbb{R}^{nN}} \sum_{i=1}^n \left(W_{\varepsilon, \boldsymbol{\mu}_i^{k+1}}^2 \right)^* (\mathbf{u}_i) \\ &\text{subject to } \sum_{i=1}^n \mathbf{u}_i = \frac{2}{\alpha} \boldsymbol{\nu}_{\text{sum}}^k. \end{aligned} \quad (49)$$

Consequently, the update (23b) can be performed by first solving the problem (49), and then evaluating the gradient of the Legendre-Fenchel conjugate (47) at the minimizer of (49).

It is known (Cuturi & Peyré, 2016, Theorem 2.4) that for given $\varepsilon > 0$ and $\boldsymbol{\mu} \in \Delta^{N-1}$, the Legendre-Fenchel conjugate $(W_{\varepsilon, \boldsymbol{\mu}}^2)^* (\mathbf{u})$ is $C^\infty(\mathbb{R}^N)$ w.r.t. $\mathbf{u} \in \mathbb{R}^N$, and the gradient $\nabla_{\mathbf{u}} (W_{\varepsilon, \boldsymbol{\mu}}^2)^* (\mathbf{u})$ is $1/\varepsilon$ Lipschitz. Furthermore, Cuturi & Peyré (2016, Theorem 2.4) gives the explicit formula

$$(W_{\varepsilon, \boldsymbol{\mu}}^2)^* (\mathbf{u}) = -\varepsilon \langle \boldsymbol{\mu}, \log(\boldsymbol{\mu} \odot (\boldsymbol{\Gamma} \exp(\mathbf{u}/\varepsilon))) \rangle, \quad (50a)$$

$$\nabla_{\mathbf{u}} (W_{\varepsilon, \boldsymbol{\mu}}^2)^* (\mathbf{u}) = \exp(\mathbf{u}/\varepsilon) \odot (\boldsymbol{\Gamma}(\boldsymbol{\mu} \odot (\boldsymbol{\Gamma} \exp(\mathbf{u}/\varepsilon)))) \in \Delta^{N-1}. \quad (50b)$$

Using (50a) in the objective of (49) followed by algebraic simplification yields (28). Using (50b) in (47), we obtain (29). \blacksquare

D Proof of Lemma 1

We re-write the constraint set \mathcal{C} as

$$\mathcal{C} = \left\{ \mathbf{z} \in \mathbb{R}^{nN} \mid \mathbf{A} \mathbf{z} = \frac{2}{\alpha} \boldsymbol{\nu}_{\text{sum}}^k \right\}, \quad (51)$$

where $\mathbf{z} = (z_1, \dots, z_n)$, $z_i \in \mathbb{R}^N$ for all $i \in [n]$, $\mathbf{A} := [\mathbf{I}_N, \dots, \mathbf{I}_N] \in \mathbb{R}^{N \times nN}$, and \mathbf{I}_N is the $N \times N$ identity matrix.

Following Bauschke & Kruk (2004, Sec. 4), we have

$$\text{proj}_{\mathcal{C}}(\mathbf{v}) = \mathbf{v} - \mathbf{A}^\dagger \left(\mathbf{A} \mathbf{v} - \frac{2}{\alpha} \boldsymbol{\nu}_{\text{sum}}^k \right) \quad (52)$$

where the superscript \dagger denotes the Moore-Penrose pseudoinverse. For our $\mathbf{A} \in \mathbb{R}^{N \times nN}$, (52) simplifies to

$$\begin{aligned} \text{proj}_{\mathcal{C}}(\mathbf{v}) &= \mathbf{v} - \mathbf{A}^\top (\mathbf{A} \mathbf{A}^\top)^{-1} \left(\mathbf{A} \mathbf{v} - \frac{2}{\alpha} \boldsymbol{\nu}_{\text{sum}}^k \right) \\ &= \mathbf{v} - \begin{bmatrix} \frac{1}{n} \mathbf{I}_N \\ \vdots \\ \frac{1}{n} \mathbf{I}_N \end{bmatrix} \left(\sum_{i=1}^n \mathbf{v}_i - \frac{2}{\alpha} \boldsymbol{\nu}_{\text{sum}}^k \right) \\ &= \mathbf{v} - \begin{bmatrix} \bar{\mathbf{v}} - \frac{2}{n\alpha} \boldsymbol{\nu}_{\text{sum}}^k \\ \vdots \\ \bar{\mathbf{v}} - \frac{2}{n\alpha} \boldsymbol{\nu}_{\text{sum}}^k \end{bmatrix}, \end{aligned}$$

thus completing the proof. \blacksquare

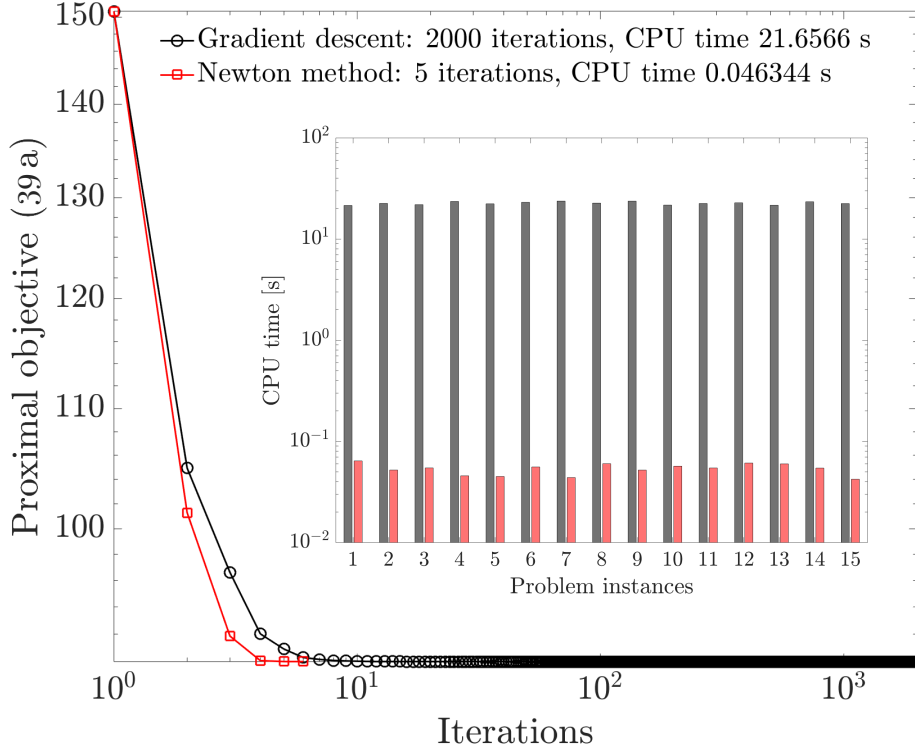


Figure 4: *Main plot*: A typical instance of the proximal optimization problem (34a) with $N = 441$, $\varepsilon = \tau = 0.1$, random initial guess, randomly generated input data (i.e., proximal argument in \mathbb{R}^N), random parameter $\mu \in \Delta^{N-1}$, and the Euclidean distance matrix $C \in \mathbb{R}^{N \times N}$ for uniform grid over $[-1, 1]^2$ with spatial discretization length 0.1 in both directions. The problem instance was solved via the gradient descent and the Newton’s method with the same numerical tolerance 10^{-4} . The stopping criterion for the gradient descent was the norm of the gradient being less than or equal to the numerical tolerance. For the Newton’s method, we used the standard stopping criterion (Boyd et al., 2004, p. 487): one half of the squared Newton decrement being less than or equal to the numerical tolerance. Both algorithms used variable step size via backtracking line search (see Appendix E) with parameters $\alpha_0 = 0.3, \beta_0 = 0.7$. For gradient descent, the proximal objective after the last iteration was equal to 90.018062265357955; the same for Newton’s method was equal to 90.018072956312977. *Inset plot*: The CPU time comparisons for 15 instances of (34a) with randomly chosen initial guess, proximal argument and parameter $\mu \in \Delta^{N-1}$ while keeping all other parameters fixed and same as before across all problem instances. The longer (resp. shorter) bars are for the gradient descent (resp. Newton’s method). For all 15 problem instances, the gradient descent took 2000–2002 iterations while the Newton’s method required 5–6 iterations. So the convergence trend shown in the main plot is typical. As explained in Sec. 4.2, solving the proximal problem (34a) arises as a sub-problem for the inner layer ADMM (34).

E Gradient and Hessian of (30), and Solving (34a)

Gradient of (30). To reduce clutter, let us drop the indices $i \in [n]$ and $k \in \mathbb{N}_0$ for the time being, and focus on computing the gradient and Hessian of

$$f(\mathbf{u}) := \langle \boldsymbol{\mu}, \log(\boldsymbol{\Gamma} \exp(\mathbf{u}/\varepsilon)) \rangle$$

w.r.t. $\mathbf{u} \in \mathbb{R}^N$ for given $\boldsymbol{\mu} = (\mu_1, \dots, \mu_N) \in \Delta^{N-1}$. Notice that f is twice continuously differentiable but is not everywhere strictly convex; e.g., f is affine along any line $\mathbf{u} = u_0 \mathbf{1}$ where u_0 is some nonzero real and $\mathbf{1}$ denotes the $N \times 1$ vector of ones.

Denote the j th row of the matrix $\boldsymbol{\Gamma} \in \mathbb{R}^{N \times N}$ as $\boldsymbol{\gamma}_j$, and write

$$f(\mathbf{u}) = \sum_{j=1}^N \mu_j \log \langle \boldsymbol{\gamma}_j, \exp(\mathbf{u}/\varepsilon) \rangle. \quad (53)$$

Using the chain rule in (53), we have

$$\nabla_{\mathbf{u}} f = \frac{1}{\varepsilon} \sum_{j=1}^N \mu_j \frac{\boldsymbol{\gamma}_j \odot \exp(\mathbf{u}/\varepsilon)}{\langle \boldsymbol{\gamma}_j, \exp(\mathbf{u}/\varepsilon) \rangle} = \frac{1}{\varepsilon} (\boldsymbol{\Gamma}^\top \boldsymbol{\mu}) \odot \exp(\mathbf{u}/\varepsilon) \odot (\boldsymbol{\Gamma} \exp(\mathbf{u}/\varepsilon)). \quad (54)$$

Bringing back the indices $i \in [n]$ and $k \in \mathbb{N}_0$ as in (30), and letting $\mathbf{e}_i := \exp(\mathbf{u}_i/\varepsilon)$, the expression (54) gives

$$\nabla_{\mathbf{u}_i} f_i = \frac{1}{\varepsilon} (\boldsymbol{\Gamma}^\top \boldsymbol{\mu}_i^{k+1}) \odot \mathbf{e}_i \odot (\boldsymbol{\Gamma} \mathbf{e}_i). \quad (55)$$

Hessian of (30). Proceeding from (55), we get the Hessian

$$\nabla_{\mathbf{u}_i}^2 f_i = \frac{1}{\varepsilon^2} \left[\text{diag} \left((\boldsymbol{\Gamma}^\top \boldsymbol{\mu}_i^{k+1}) \odot \mathbf{e}_i \odot (\boldsymbol{\Gamma} \mathbf{e}_i) \right) - \text{diag} \left((\boldsymbol{\Gamma}^\top \boldsymbol{\mu}_i^{k+1}) \odot (\boldsymbol{\Gamma} \mathbf{e}_i)^2 \right) \boldsymbol{\Gamma} \odot (\mathbf{e}_i \mathbf{e}_i^\top) \right] \quad (56)$$

where $(\boldsymbol{\Gamma} \mathbf{e}_i)^2$ denotes the elementwise square of the vector $\boldsymbol{\Gamma} \mathbf{e}_i$.

Because the matrix \mathbf{C} is symmetric, $\boldsymbol{\Gamma}$ is symmetric too, and we can drop the transpose from (56). Furthermore, since $\boldsymbol{\Gamma} \odot (\mathbf{e}_i \mathbf{e}_i^\top) = \text{diag}(\mathbf{e}_i) \boldsymbol{\Gamma} \text{diag}(\mathbf{e}_i)$, we can rewrite (56) as

$$\nabla_{\mathbf{u}_i}^2 f_i = \frac{1}{\varepsilon^2} \text{diag} \left((\boldsymbol{\Gamma} \boldsymbol{\mu}_i^{k+1}) \odot \mathbf{e}_i \odot (\boldsymbol{\Gamma} \mathbf{e}_i) \right) [\mathbf{I}_N - \text{diag}(\mathbf{1} \odot (\boldsymbol{\Gamma} \mathbf{e}_i)) \boldsymbol{\Gamma} \text{diag}(\mathbf{e}_i)]. \quad (57)$$

Notice that the matrix $\text{diag}(\mathbf{1} \odot (\boldsymbol{\Gamma} \mathbf{e}_i)) \boldsymbol{\Gamma} \text{diag}(\mathbf{e}_i)$ is elementwise positive and row stochastic, and therefore, by linear Perron-Frobenius theorem, the matrix in square braces in (57) has zero as a simple eigenvalue. Thus, the Hessian (57) is positive semidefinite. The Hessian of the proximal objective in (34a) is $\mathbf{I}_N + \frac{1}{\tau} \nabla_{\mathbf{u}_i}^2 f_i$ where $\tau > 0$, and is, therefore, strictly positive definite.

Solving (34a) via Newton's Method. The structured Hessian of the proximal objective in (34a) mentioned above, makes the per iteration complexity for solving (34a) via Newton's method to be $\mathcal{O}(N^2)$ flops instead of $\mathcal{O}(N^3)$ flops—the latter would be the case for Cholesky factorization-based solution of the associated linear system. Fig. 4 shows that the typical convergence for the Newton's method occurs in approx. 5 iterations, much faster than gradient descent (see Fig. 4 caption for details).

Backtracking line search. For unconstrained minimization of an objective f_0 via recursive algorithms such as gradient descent or Newton's method, at each iteration, we compute the corresponding descent direction Δx at $x \in \text{domain}(f_0)$. Then we apply the recursive update rule $x \leftarrow x + t \Delta x$ where t is a variable step size at that iteration. A standard method of computing the step size is the backtracking line search (Boyd et al., 2004, p. 464). Given parameters $\alpha_0 \in (0, 0.5)$, $\beta_0 \in (0, 1)$, the backtracking line search starts with an initial step size $t = 1$, and while $f_0(x + t \Delta x) > f_0(x) + \alpha_0 t \langle \nabla f, \Delta x \rangle$, sets $t \leftarrow \beta_0 t$. The resulting value of t is used as the step size at that iteration. Both the gradient descent and Newton's method implementations as reported in Fig. 4, use backtracking line search with parameter values detailed in Fig. 4 caption.

Lemma 3. *The C^2 convex function f given by (53) with $\text{domain}(f) = \mathbb{R}^N$, has Lipschitz continuous gradient w.r.t. $\|\cdot\|_2$ with Lipschitz constant $L = \frac{1}{\varepsilon^2} \|\mathbf{\Gamma} \boldsymbol{\mu}^{k+1}\|_\infty$.*

Proof. Let $\mathbf{e} := \exp(\mathbf{u}/\varepsilon)$. From (56), for all $\mathbf{u}, \mathbf{v} \in \mathbb{R}^N$, we have

$$\begin{aligned} \mathbf{v}^\top \nabla^2 f(\mathbf{u}) \mathbf{v} &= \frac{1}{\varepsilon^2} \mathbf{v}^\top \left[\text{diag} \left((\mathbf{\Gamma}^\top \boldsymbol{\mu}^{k+1}) \odot \mathbf{e} \otimes (\mathbf{\Gamma} \mathbf{e}) \right) - \text{diag} \left((\mathbf{\Gamma}^\top \boldsymbol{\mu}^{k+1}) \otimes (\mathbf{\Gamma} \mathbf{e})^2 \right) \mathbf{\Gamma} \odot (\mathbf{e} \mathbf{e}^\top) \right] \mathbf{v} \\ &\leq \frac{1}{\varepsilon^2} \mathbf{v}^\top \text{diag} \left((\mathbf{\Gamma}^\top \boldsymbol{\mu}^{k+1}) \odot \mathbf{e} \otimes (\mathbf{\Gamma} \mathbf{e}) \right) \mathbf{v}, \end{aligned} \quad (58)$$

since the quadratic term followed by the minus sign is nonnegative. Hence (58) yields

$$\mathbf{v}^\top \nabla^2 f(\mathbf{u}) \mathbf{v} \leq \frac{1}{\varepsilon^2} \left\| (\mathbf{\Gamma}^\top \boldsymbol{\mu}^{k+1}) \odot \mathbf{e} \otimes (\mathbf{\Gamma} \mathbf{e}) \right\|_\infty \|\mathbf{v}\|_2^2 \leq \frac{1}{\varepsilon^2} \|\mathbf{\Gamma}^\top \boldsymbol{\mu}^{k+1}\|_\infty \|\mathbf{e} \otimes (\mathbf{\Gamma} \mathbf{e})\|_\infty \|\mathbf{v}\|_2^2. \quad (59)$$

Recall that $\mathbf{\Gamma} := \exp(-\mathbf{C}/2\varepsilon)$ where $\mathbf{C} \in \mathbb{R}^{N \times N}$ is a squared Euclidean distance matrix. So the entries of the symmetric matrix \mathbf{C} are in $[0, \infty)$ and thus, the entries of the symmetric matrix $\mathbf{\Gamma}$ are in $(0, 1]$ with all diagonal entries being equal to 1. Therefore, $\|\mathbf{e} \otimes (\mathbf{\Gamma} \mathbf{e})\|_\infty \leq 1$, and (59) gives

$$\mathbf{v}^\top \nabla^2 f(\mathbf{u}) \mathbf{v} \leq \frac{1}{\varepsilon^2} \|\mathbf{\Gamma} \boldsymbol{\mu}^{k+1}\|_\infty \|\mathbf{v}\|_2^2 \quad \forall \mathbf{u}, \mathbf{v} \in \mathbb{R}^N,$$

where we dropped the transpose due to the symmetry of $\mathbf{\Gamma}$. Invoking Lemma 2, we conclude the proof. \blacksquare

Theorem 4. *Let \mathbf{C} , $\mathbf{\Gamma}$, and $\boldsymbol{\mu}_i^{k+1} \in \Delta^{N-1}$ for all $i \in [n]$, $k \in \mathbb{N}_0$, as in Theorem 1. If*

$$\tau > \frac{\sqrt{2}}{\varepsilon^2} \|\mathbf{\Gamma} \boldsymbol{\mu}_n^{k+1}\|_\infty, \quad (60)$$

then the sequence $(\mathbf{u}_1^\ell, \dots, \mathbf{u}_n^\ell)$ generated by the inner layer ADMM given in (34) converge to the optimal solutions of problem (28), i.e., $(\mathbf{u}_1^\ell, \dots, \mathbf{u}_n^\ell) \xrightarrow{\ell \nearrow \infty} (\mathbf{u}_1^{\text{opt}}, \dots, \mathbf{u}_n^{\text{opt}})$.

Proof. We start our proof by presenting a sufficient condition for convergence of certain generic multi-block ADMM, and show that the inner layer ADMM given in (34) satisfies these conditions.

To this end, we start with the following convex minimization problem:

$$\begin{aligned} &\min_{(\mathbf{u}_1, \dots, \mathbf{u}_n) \in \mathbb{R}^{nN}} g_1(\mathbf{u}_1) + g_2(\mathbf{u}_2) + \dots + g_n(\mathbf{u}_n) \\ &\text{subject to } \mathbf{A}_1 \mathbf{u}_1 + \mathbf{A}_2 \mathbf{u}_2 + \dots + \mathbf{A}_n \mathbf{u}_n = \mathbf{b}, \\ &\quad \mathbf{u}_i \in \mathcal{U}_i \quad \text{for all } i \in [n], \end{aligned} \quad (61)$$

where $\mathbf{A}_i \in \mathbb{R}^{N \times N}$, $\mathbf{b} \in \mathbb{R}^N$, the sets $\mathcal{U}_i \subseteq \mathbb{R}^N$ are closed convex, and $g_i : \mathcal{U}_i \rightarrow \mathbb{R}$ are closed convex functions for all $i \in [n]$. The augmented Lagrangian for (61) is

$$\mathcal{L}_\tau(\mathbf{u}_1, \dots, \mathbf{u}_n; \boldsymbol{\lambda}) := g_1(\mathbf{u}_1) + \dots + g_n(\mathbf{u}_n) + \left\langle \boldsymbol{\lambda}, \sum_{i=1}^n \mathbf{A}_i \mathbf{u}_i - \mathbf{b} \right\rangle + \frac{\tau}{2} \left\| \sum_{i=1}^n \mathbf{A}_i \mathbf{u}_i - \mathbf{b} \right\|^2, \quad (62)$$

where $\boldsymbol{\lambda} \in \mathbb{R}^N$ is the Lagrange multiplier, and $\tau > 0$ is a penalty parameter. For (61), consider the multi-block ADMM recursions:

$$\begin{cases} \mathbf{u}_1^{\ell+1} = \underset{\mathbf{u}_1 \in \mathcal{U}_1}{\text{argmin}} \mathcal{L}_\tau(\mathbf{u}_1, \mathbf{u}_2^\ell, \dots, \mathbf{u}_n^\ell; \boldsymbol{\lambda}^\ell), \\ \mathbf{u}_2^{\ell+1} = \underset{\mathbf{u}_2 \in \mathcal{U}_2}{\text{argmin}} \mathcal{L}_\tau(\mathbf{u}_1^{\ell+1}, \mathbf{u}_2, \mathbf{u}_3^\ell, \dots, \mathbf{u}_n^\ell; \boldsymbol{\lambda}^\ell), \\ \vdots \\ \mathbf{u}_n^{\ell+1} = \underset{\mathbf{u}_n \in \mathcal{U}_n}{\text{argmin}} \mathcal{L}_\tau(\mathbf{u}_1^{\ell+1}, \mathbf{u}_2^{\ell+1}, \dots, \mathbf{u}_{n-1}^{\ell+1}, \mathbf{u}_n; \boldsymbol{\lambda}^\ell), \\ \boldsymbol{\lambda}^{\ell+1} = \boldsymbol{\lambda}^\ell + \tau \left(\sum_{i=1}^n \mathbf{A}_i \mathbf{u}_i^{\ell+1} - \mathbf{b} \right). \end{cases} \quad (63)$$

For (61), when the following conditions (Hong et al., 2016, Corollary 3.5):

- c1. the matrices \mathbf{A}_i have full column rank for all $i \in [n-1]$, and $\mathbf{A}_n = \mathbf{I}_N$,
- c2. the sets \mathcal{U}_i are closed convex for all $i \in [n]$,
- c3. the mappings g_i are lower bounded for all $i \in [n]$,
- c4. $\tau > \sqrt{2}L$ where L is Lipschitz constant (w.r.t. $\|\cdot\|_2$) for $\nabla_{\mathbf{u}_n} g_n$,

are satisfied, then as the recursion index $\ell \nearrow \infty$, the solution of the multi-block ADMM (63) converges to the optimal solutions of (61). Notice that the recursions (34) associated with the problem (28), are indeed an instance of the generic recursions (63) associated with (61). In particular,

$$g_i(\mathbf{u}_i) \equiv \langle \boldsymbol{\mu}_i^{k+1}, \log(\mathbf{\Gamma} \exp(\mathbf{u}_i/\varepsilon)) \rangle,$$

where the probability vectors $\boldsymbol{\mu}_i^{k+1} \in \Delta^{N-1}$ for all $i \in [n]$, $k \in \mathbb{N}_0$. Thus motivated, we check the conditions c1-c4.

Specifically, condition c1 for (28) is satisfied because $\mathbf{A}_i = \mathbf{I}_N$ for all $i \in [n]$. Condition c2 for (28) holds since $\mathcal{U}_i = \mathbb{R}^N$ for all $i \in [n]$, which are closed as well as affine (hence convex) sets.

For condition c3, we need to verify that the mappings $\mathbf{u}_i \mapsto g_i(\mathbf{u}_i) = \langle \boldsymbol{\mu}_i^{k+1}, \log(\mathbf{\Gamma} \exp(\mathbf{u}_i/\varepsilon)) \rangle$ are uniformly lower bounded. The lower bound for $\mathbf{u}_i \mapsto g_i(\mathbf{u}_i)$ can be found as the following unconstrained minimum

$$g_i^{\text{opt}} := \min_{\mathbf{u}_i \in \mathbb{R}^N} \langle \boldsymbol{\mu}_i^{k+1}, \log(\mathbf{\Gamma} \exp(\mathbf{u}_i/\varepsilon)) \rangle, \quad (64)$$

which is the minimum of a convex combination of log-sum-exp composed with an affine map.

By choosing matrix \mathbf{A} as an invertible matrix and introducing two new variables, $\tilde{\mathbf{u}} \in \mathbb{R}^N$ and $\mathbf{y} \in \mathbb{R}^N$, we reformulate problem (64) as:

$$\begin{aligned} \min_{\mathbf{y} \in \mathbb{R}^N} f_0(\mathbf{y}) &:= \mu_j \log \sum_{i=1}^N \exp(\mathbf{y}_i) \\ \text{subject to } \mathbf{u}/\varepsilon &= \mathbf{A}\tilde{\mathbf{u}}, \\ \mathbf{A}\tilde{\mathbf{u}} + \log \boldsymbol{\gamma}_j &= \mathbf{y}, \end{aligned} \quad (65)$$

where \mathbf{y}_i is i th element of vector \mathbf{y} . The Lagrangian of the reformulated problem is

$$L(\mathbf{u}, \tilde{\mathbf{u}}, \mathbf{y}, \boldsymbol{\kappa}, \boldsymbol{\eta}) = \mu_j \log \sum_{i=1}^N \exp(\mathbf{y}_i) + \boldsymbol{\eta}^\top (\mathbf{A}\tilde{\mathbf{u}} + \log \boldsymbol{\gamma}_j - \mathbf{y}) + \boldsymbol{\kappa}^\top (\mathbf{u}/\varepsilon - \mathbf{A}\tilde{\mathbf{u}}), \quad (66)$$

where $\boldsymbol{\kappa}$ and $\boldsymbol{\eta}$ are the Lagrangian multipliers, and the corresponding Lagrange dual function is defined as

$$h(\boldsymbol{\eta}, \boldsymbol{\kappa}) = \inf_{\mathbf{u}, \tilde{\mathbf{u}}, \mathbf{y}} \left\{ \mu_j \log \sum_{i=1}^N \exp(\mathbf{y}_i) + \boldsymbol{\eta}^\top (\mathbf{A}\tilde{\mathbf{u}} + \log \boldsymbol{\gamma}_j - \mathbf{y}) + \boldsymbol{\kappa}^\top (\mathbf{u}/\varepsilon - \mathbf{A}\tilde{\mathbf{u}}) \right\}. \quad (67)$$

Minimizing over \mathbf{u} results in $h(\boldsymbol{\eta}, \boldsymbol{\kappa}) = -\infty$ unless $\boldsymbol{\kappa} = \mathbf{0}$. Substituting $\boldsymbol{\kappa} = \mathbf{0}$ in (67), we get

$$h(\boldsymbol{\eta}) = \inf_{\tilde{\mathbf{u}}, \mathbf{y}} \left(\mu_j \log \sum_{i=1}^N \exp(\mathbf{y}_i) + \boldsymbol{\eta}^\top (\mathbf{A}\tilde{\mathbf{u}} + \log \boldsymbol{\gamma}_j - \mathbf{y}) \right). \quad (68)$$

Minimizing over $\tilde{\mathbf{u}}$ results in $h(\boldsymbol{\eta}) = -\infty$ unless $\mathbf{A}^\top \boldsymbol{\eta} = \mathbf{0}$. So,

$$h(\boldsymbol{\eta}) = \boldsymbol{\eta}^\top \log \boldsymbol{\gamma}_j + \inf_{\mathbf{y}} \left(\mu_j \log \sum_{i=1}^N \exp(\mathbf{y}_i) - \boldsymbol{\eta}^\top \mathbf{y} \right) = \boldsymbol{\eta}^\top \log \boldsymbol{\gamma}_j + f_0^*(\boldsymbol{\eta}), \quad (69)$$

where the conjugate of f_0 is

$$f_0^* = \begin{cases} \left\langle \boldsymbol{\eta}, \log \frac{\boldsymbol{\eta}}{\mu_j} \right\rangle & \boldsymbol{\eta} \succeq 0, \mathbf{1}^\top \boldsymbol{\eta} = 1, \\ \infty & \text{otherwise.} \end{cases} \quad (70)$$

Therefore, the dual problem of (65) is

$$\begin{aligned} & \max_{\boldsymbol{\eta} \in \mathbb{R}^N} \boldsymbol{\eta}^\top \log \boldsymbol{\gamma}_j - \left\langle \boldsymbol{\eta}, \log \frac{\boldsymbol{\eta}}{\boldsymbol{\mu}_j} \right\rangle \\ & \text{subject to } \boldsymbol{\eta} \succeq 0, \\ & \quad \mathbf{1}^\top \boldsymbol{\eta} = 1, \\ & \quad \mathbf{A}^\top \boldsymbol{\eta} = 0. \end{aligned} \tag{71}$$

The solution to the above entropy maximization problem provides a lower bound for the mappings $\mathbf{u} \mapsto \mu_j \log \langle \boldsymbol{\gamma}_j, \exp(\mathbf{u}/\varepsilon) \rangle$ in \mathbb{R}^N , thus helping satisfy condition c3.

From Lemma 3, $\nabla_{\mathbf{u}_n} g_n$ has the Lipschitz constant $L = \frac{1}{\varepsilon^2} \|\mathbf{\Gamma}^\top \boldsymbol{\mu}^{k+1}\|_\infty$. So, by choosing

$$\tau > \frac{\sqrt{2}}{\varepsilon^2} \|\mathbf{\Gamma}^\top \boldsymbol{\mu}^{k+1}\|_\infty$$

we satisfy condition c4. This completes the proof. \blacksquare

H Details of the Aggregation-Drift-Diffusion Nonlinear PDE Case Study

We choose four different ways of splitting the spatial operators of this nonlinear PDE and present the simulation results for each case of splitting. These choices lead to differently split free energy functionals in our proposed two-layer ADMM, and it is natural to investigate comparative numerical performance due to such variability.

In the first case, we group $\nabla \cdot (\mu \nabla (U \circledast \mu))$ and $\nabla \cdot (\mu \nabla V)$ together as the first term, and $\beta^{-1} \Delta \mu^2$ as the second term:

$$\frac{\partial \mu}{\partial t} = \underbrace{\nabla \cdot (\mu \nabla V)}_{i=1} + \beta^{-1} \Delta \mu^2 + \underbrace{\nabla \cdot (\mu \nabla U \circledast \mu)}_{i=2}.$$

In the second case, we group $\nabla \cdot (\mu \nabla (U \circledast \mu))$ and $\beta^{-1} \Delta \mu^2$ together as the first term, and $\nabla \cdot (\mu \nabla V)$ as the second term:

$$\frac{\partial \mu}{\partial t} = \underbrace{\nabla \cdot (\mu \nabla U \circledast \mu)}_{i=1} + \beta^{-1} \Delta \mu^2 + \underbrace{\nabla \cdot (\mu \nabla V)}_{i=2}.$$

In the third case, we group $\nabla \cdot (\mu \nabla U \circledast \mu)$ and $\nabla \cdot (\mu \nabla V)$ together as the first term, and $\beta^{-1} \Delta \mu^2$ as the second term:

$$\frac{\partial \mu}{\partial t} = \underbrace{\nabla \cdot (\mu \nabla V)}_{i=1} + \underbrace{\nabla \cdot (\mu \nabla U \circledast \mu)}_{i=2} + \underbrace{\beta^{-1} \Delta \mu^2}_{i=3}.$$

Finally, in the fourth case, we consider $\nabla \cdot (\mu \nabla U \circledast \mu)$ as the first term, $\nabla \cdot (\mu \nabla V)$ as the second term, and $\beta^{-1} \Delta \mu^2$ as the third term:

$$\frac{\partial \mu}{\partial t} = \underbrace{\nabla \cdot (\mu \nabla V)}_{i=1} + \underbrace{\nabla \cdot (\mu \nabla U \circledast \mu)}_{i=2} + \underbrace{\beta^{-1} \Delta \mu^2}_{i=3}.$$

The corresponding F_i 's and the pairwise Wasserstein distances between the solutions $\boldsymbol{\mu}_i^k$ and $\boldsymbol{\mu}_j^k$, $i \neq j$, for each case of splitting are given in Table 2. The reported Wasserstein distances are computed by solving the respective Kantorovich linear programs. Table 3 shows a comparison between how long it took for the centralized and proposed Wasserstein ADMM methods to run using the same simulation setup. It also displays the accuracy results by plotting the Wasserstein distances between the centralized and Wasserstein ADMM iterations, based on the known stationary measure. These results provide two clear findings: Firstly, the proposed ADMM updates are faster (much faster when using three-way splitting) than the corresponding updates in the centralized approach. Secondly, as the iterations continue, the proposed algorithm outperforms the centralized method in terms of

Case	Functionals	Wasserstein distances
#1	$F_1(\boldsymbol{\mu}) = \langle \mathbf{V}_k + \beta^{-1} \boldsymbol{\mu}, \boldsymbol{\mu} \rangle,$ $F_2(\boldsymbol{\mu}) = \langle \mathbf{U}_k \boldsymbol{\mu}^k, \boldsymbol{\mu} \rangle$ average runtime = 294.06 s	
#2	$F_1(\boldsymbol{\mu}) = \langle \mathbf{U}_k \boldsymbol{\mu}^k + \beta^{-1} \boldsymbol{\mu}, \boldsymbol{\mu} \rangle,$ $F_2(\boldsymbol{\mu}) = \langle \mathbf{V}_k, \boldsymbol{\mu} \rangle$ average runtime = 285.32 s	
#3	$F_1(\boldsymbol{\mu}) = \langle \mathbf{U}_k \boldsymbol{\mu}^k + \mathbf{V}_k, \boldsymbol{\mu} \rangle,$ $F_2(\boldsymbol{\mu}) = \langle \beta^{-1} \boldsymbol{\mu}, \boldsymbol{\mu} \rangle$ average runtime = 289.87 s	
#4	$F_1(\boldsymbol{\mu}) = \langle \mathbf{V}_k, \boldsymbol{\mu} \rangle,$ $F_2(\boldsymbol{\mu}) = \langle \mathbf{U}_k \boldsymbol{\mu}^k, \boldsymbol{\mu} \rangle,$ $F_3(\boldsymbol{\mu}) = \langle \beta^{-1} \boldsymbol{\mu}, \boldsymbol{\mu} \rangle$ average runtime = 108.99 s	

Table 2: For the aggregation-drift-diffusion nonlinear PDE, the choice of functionals F_i , $i \in \{1, 2, 3\}$ for each case of splitting and the pairwise Wasserstein distances between the solutions $\boldsymbol{\mu}_i^k$ and $\boldsymbol{\mu}_j^k$, $i, j \in \{1, 2, 3\}$, $i \neq j$, for 100 executions of the code with the same initial samples. In the functional column, the drift potential vector $\mathbf{V}_k \in \mathbb{R}^N$ and the symmetric matrix $\mathbf{U}_k \in \mathbb{R}^{N \times N}$ are respectively given by $\mathbf{V}_k(i) := V(\boldsymbol{\theta}_k^i)$, $i \in [N]$ and $\mathbf{U}_k(i, j) := U(\boldsymbol{\theta}_k^i - \boldsymbol{\theta}_k^j)$, $i, j \in [N]$. We executed the code for each case of splitting 100 times and plot the averaged Wasserstein distance for each splitting case. The figures in the first three rows show the averaged Wasserstein distance of the solution of each term after 10000 iterations for the cases that we split the nonlinear PDE to two terms, and the shadow shows the variation range for each case of splitting. In the last row, each curve shows the averaged Wasserstein distance of the solution of each term after 10000 iterations for the cases that we split the nonlinear PDE to three terms. The shadow shows the variation range of each Wasserstein distances of $\boldsymbol{\mu}_1$, $\boldsymbol{\mu}_2$, and $\boldsymbol{\mu}_3$. Because we start from the same initial distribution for $\boldsymbol{\mu}_i$, $i = \{1, 2, 3\}$, $W(\boldsymbol{\mu}_i^k, \boldsymbol{\mu}_j^k)$, $i, j \in \{1, 2, 3\}$, $i \neq j$ at $k = 0$ is zero. In the reported average runtimes, the average is taken over the 100 executions of the same code with the same initial samples.

accuracy, as seen in the improvement of Wasserstein distance to the known stationary solution. In Table 4, we show how the final objective value changes for this case study based on different ADMM barrier parameter values (α). We maintained a constant inner ADMM iteration number of 3 throughout this analysis. We also performed simulations varying the inner ADMM iteration number while keeping $\alpha = 12$ fixed. The resulting fluctuations in the final objective value are detailed in Table 5.

I Grouping of Summand Functionals

In (1), $F = F_1 + \dots + F_n$, $n > 1$, where the summand functionals F_i , $i \in [n]$, are necessarily *distinct*. Suppose that we have n *indistinguishable* computing elements available for distributed computation. We can use any subset of them to implement our proposed algorithm depending on how we group the n distinct summand functionals. Clearly, the grouping $\{\{F_1, \dots, F_n\}, \{0\}, \dots, \{0\}\}$

Case	Functionals	Wasserstein distances
#1	$F_1(\boldsymbol{\mu}) = \langle \mathbf{V}_k + \beta^{-1}\boldsymbol{\mu}, \boldsymbol{\mu} \rangle,$ $F_2(\boldsymbol{\mu}) = \langle \mathbf{U}_k \boldsymbol{\mu}^k, \boldsymbol{\mu} \rangle$	
#2	$F_1(\boldsymbol{\mu}) = \langle \mathbf{U}_k \boldsymbol{\mu}^k + \beta^{-1}\boldsymbol{\mu}, \boldsymbol{\mu} \rangle,$ $F_2(\boldsymbol{\mu}) = \langle \mathbf{V}_k, \boldsymbol{\mu} \rangle$	
#3	$F_1(\boldsymbol{\mu}) = \langle \mathbf{U}_k \boldsymbol{\mu}^k + \mathbf{V}_k, \boldsymbol{\mu} \rangle,$ $F_2(\boldsymbol{\mu}) = \langle \beta^{-1}\boldsymbol{\mu}, \boldsymbol{\mu} \rangle$	
#4	$F_1(\boldsymbol{\mu}) = \langle \mathbf{V}_k, \boldsymbol{\mu} \rangle,$ $F_2(\boldsymbol{\mu}) = \langle \mathbf{U}_k \boldsymbol{\mu}^k, \boldsymbol{\mu} \rangle,$ $F_3(\boldsymbol{\mu}) = \langle \beta^{-1}\boldsymbol{\mu}, \boldsymbol{\mu} \rangle$	

Table 3: For the aggregation-drift-diffusion nonlinear PDE case study in Sec. V, comparison of the Wasserstein distances to the known stationary solution $\boldsymbol{\mu}_\infty$, from the iterates of the centralized ($\boldsymbol{\mu}^k_{\text{centralized}}$), and from the iterates of the proposed Wasserstein ADMM algorithm $\boldsymbol{\mu}_i^k$, $i = 1, 2, 3$. The known $\boldsymbol{\mu}_\infty$ here is a uniform measure over an annulus with the inner radius $R_i = 1/2$ and the outer radius $R_o = \sqrt{5}/2$ (Carrillo et al., 2022, Sec. 4.3.2). All Wasserstein distances are computed by solving the corresponding Kantorovich LPs as in Supp. Material Sec. H, Table 2. All simulations are done with the same set up as in Sec. V and Supp. Material H, Table 2, i.e., with the same uniform grid over $[-2, 2]^2$ with 1681 samples, $\beta^{-1} = 0.0520$ as in (Carrillo et al., 2022, Sec. 4.3.2), and the same μ_0, U, V and other parameters reported in Sec. V. For centralized computation, we used the proximal recursion algorithm in (Caluya & Halder, 2019). The figures in the last column show that after 10000 iterations, the Wasserstein distances between μ_i and μ_∞ in all cases are smaller than the corresponding Wasserstein distance between the centralized solution and μ_∞ . The average runtime (averaged over 100 executions of the same code as in Table 2, Supp. Material) from the proposed Wasserstein ADMM algorithm in all cases remain below 300 sec, and especially it is recorded at 108.99 sec in case #4, significantly below the total runtime of the centralized variant (310.21 sec).

α	10	10.5	11	11.5	12	12.5	13	13.5	14	14.5	15
F^{10000} , case #1	10.8945	10.9153	10.9058	10.9224	10.8978	10.9064	10.8922	10.9203	10.9124	10.9203	10.9139
F^{10000} , case #2	11.0544	11.0586	11.0624	11.0598	11.0618	11.0578	11.0694	11.0692	11.0591	11.0570	11.0561
F^{10000} , case #3	11.0282	11.0344	11.0296	11.0325	11.0275	11.0312	11.0338	11.0301	11.0395	11.0351	11.0305
F^{10000} , case #4	16.5034	16.5051	16.5087	16.5012	16.5106	16.5080	16.5049	16.5029	16.5030	16.5018	16.5057

Table 4: Value of the objective $F^{10000} := \langle \mathbf{V}_k + \mathbf{U}_k \boldsymbol{\mu}^k + \beta^{-1}\boldsymbol{\mu}, \boldsymbol{\mu} \rangle|_{k=10000}$ at the final consensus iterate $\boldsymbol{\mu} \equiv \boldsymbol{\mu}^{10000}$ for cases in Fig. 1 w.r.t. different values of ADMM barrier parameter $\alpha \in [10, 15]$.

Inner layer ADMM iter. #	3	4	5	6	7	8	9	10
F^{10000} , case #1	10.9263	10.8981	10.9165	10.8997	10.9124	10.9157	10.8813	10.9009
F^{10000} , case #2	11.0638	11.0546	11.0643	11.0625	11.0632	11.0583	11.0701	11.0678
F^{10000} , case #3	11.0368	11.0457	11.0374	11.0381	11.0363	11.0359	11.0318	11.0322
F^{10000} , case #4	16.5072	16.5023	16.5046	16.5001	16.5123	16.5039	16.5045	16.5034

Table 5: Value of the objective $F^{10000} := \langle \mathbf{V}_k + \mathbf{U}_k \boldsymbol{\mu}^k + \beta^{-1}\boldsymbol{\mu}, \boldsymbol{\mu} \rangle|_{k=10000}$ at the final consensus iterate $\boldsymbol{\mu} \equiv \boldsymbol{\mu}^{10000}$ for cases in Fig. 1 w.r.t. different number for the Inner layer ADMM iteration.

corresponds to centralized computation. Then the number of ways to implement our distributed algorithm over n computing elements is

$$B_n - 1, \quad n = 2, 3, \dots, \quad \text{where } B_n \text{ denotes the } n\text{th Bell number (Bell, 1938).} \quad (72)$$

The minus one in (72) discounts the centralized computation. The first few Bell numbers are $B_2 = 2, B_3 = 5, B_4 = 15, B_5 = 52, B_6 = 203, \dots$

For our first experiment in Sec. 5, $n = 2$ and there is $B_2 - 1 = 1$ way to implement the proposed algorithm. For our second experiment in Sec. 5, $n = 3$ and there are $B_3 - 1 = 4$ ways to implement the proposed algorithm as detailed in Appendix H.

More generally, if we have n distinct summand functionals with $r \leq n$ indistinguishable computing elements available, then the number of ways to implement our distributed algorithm is

$$\sum_{k=1}^r \left\{ \begin{matrix} n \\ k \end{matrix} \right\}, \quad \text{where } \left\{ \begin{matrix} n \\ k \end{matrix} \right\} \text{ denote the Stirling numbers of second kind (Graham et al., 1988, p. 244).} \quad (73)$$

For $r = n$, (73) reduces to (72).